# Study of direct photon production in Pb-Pb collisions at $\sqrt{s_{NN}} = 5.02$ TeV with ALICE experiment's Photon Spectrometer(PHOS) at Large Hadron Collider

Sushobhan Kumar Mandal

National Center for Nuclear Research

*Warsaw, Poland*

January 23, 2025

# Overview

# Strong interaction and some features of QCD

# Standard model and strong interaction

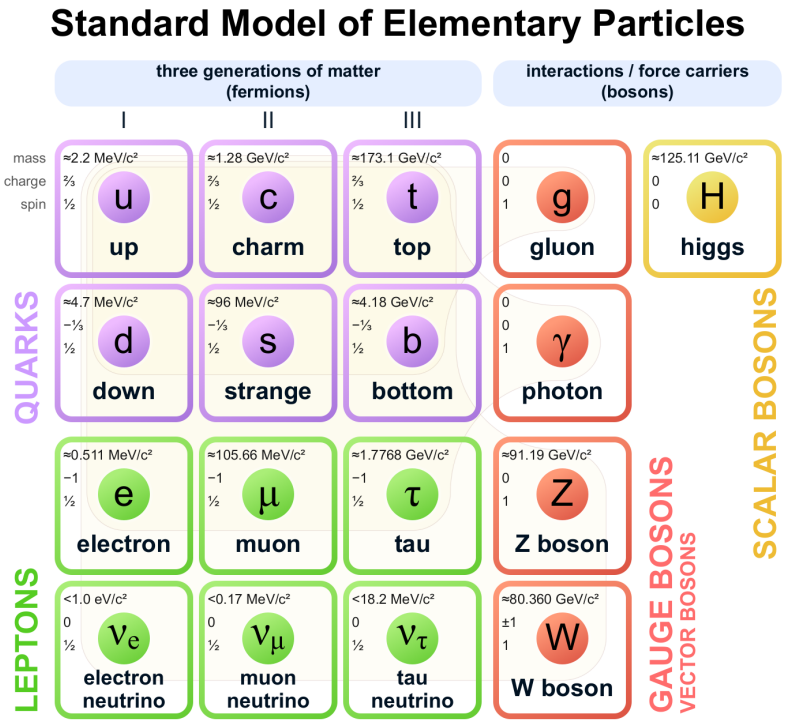


Figure: Standard model of particle physics [1]

- Quarks and Gluons carry three types of **color charges**(RGB)
- **Gluons** act as mediators between the quarks resulting strong interaction
- **Bound states** of quarks are formed resulting ordinary matter(baryons, mesons and others) around us

Strength Comparison The **strong force**[range: $10^{-15}$m] is hundred($\sim$137) times stronger than the *electromagnetic force*[range: $\infty$]
and million times($\sim 10^6$) stronger than the *weak force*[range: $10^{-18}$m]

[1] Image source: [wikipedia]

# Features of Quantum Chromodynamics(QCD)

- Color confinement: **Free color charges do not exist** in the nature
- Chiral symmetry breaking: $\sim$**99% of the proton's mass**(938 MeV) comes from **QCD interaction** rather than the masses of quarks(10 MeV)
- Asymptotic freedom: Quarks and gluons behave like **free particles** at very **high interaction energies**. This enables us to apply perturbation theory in QCD(**pQCD**)

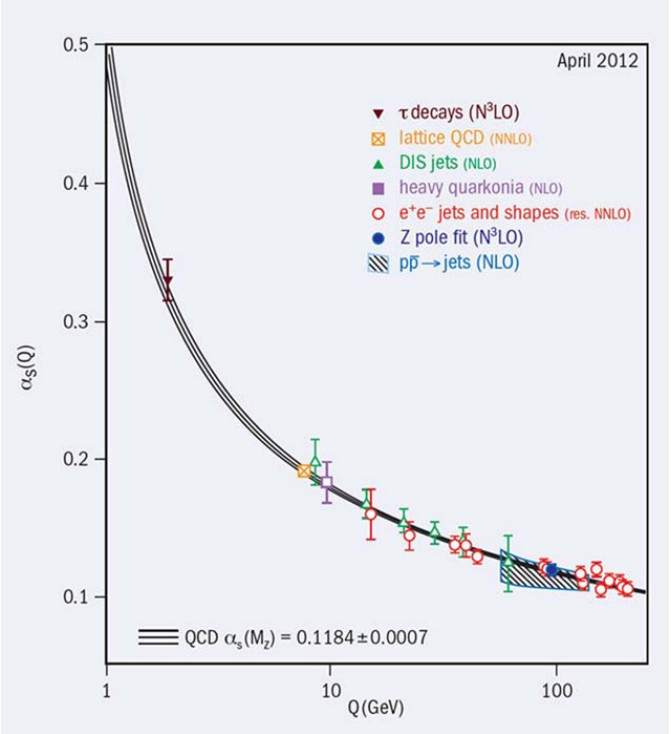


Figure: $\alpha_s(Q^2) = \frac{4\pi}{\beta_0 \times ln(Q^2/\Lambda^2)}$, the effective coupling strength decreases as a function of increasing interaction energy(Q) or decreasing distance [2].
(Gross, Wilczek and Politzer received **Nobel Prize in 2004** for Asymptotic freedom in in QCD)

[2] Figure 3 in Siegfried Bethke "World Summary of $\alpha_s$ (2012)" MPP-2012-132 arXiv:1210.0325 [hep-ex].

# Phase transition in QCD and Quark-gluon plasma(QGP)

- By **increasing the energy density (∼1 GeV/$fm^3$)** [3]over a large volume
- or, **heating to high temperature (∼170 MeV)** [4](or both),

  the hadronic matter is expected to enter a **deconfined state** of asymptotically-free quarks and gluons, exhibiting ***fluid-like phase***

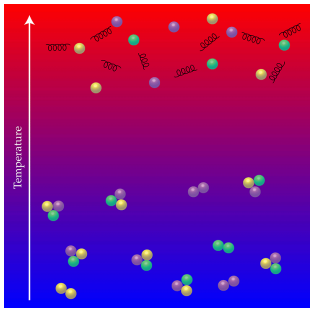


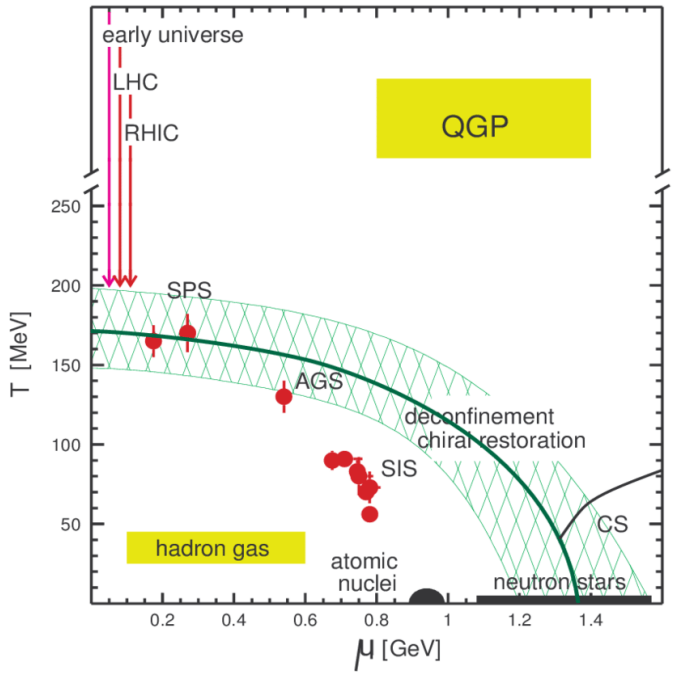


Figure: QCD Phase diagram : Several experiments have probed and still probing different regions of the phase diagram to understand the collective properties of quarks and gluons in various situations

- Lattice QCD loses its applicability at finite $\mu_B$(sign problem). The phase diagram has to be explored by **comparing experimental results with effective models**

[3]Karsch, Lect. Notes Phys., 209 (2002), hep-lat/0106019; [4]Borsanyi et al., JHEP 1009 (2010) 073 [arXiv:1005.3508[hep-lat]]

# Early universe and Quark deconfinement

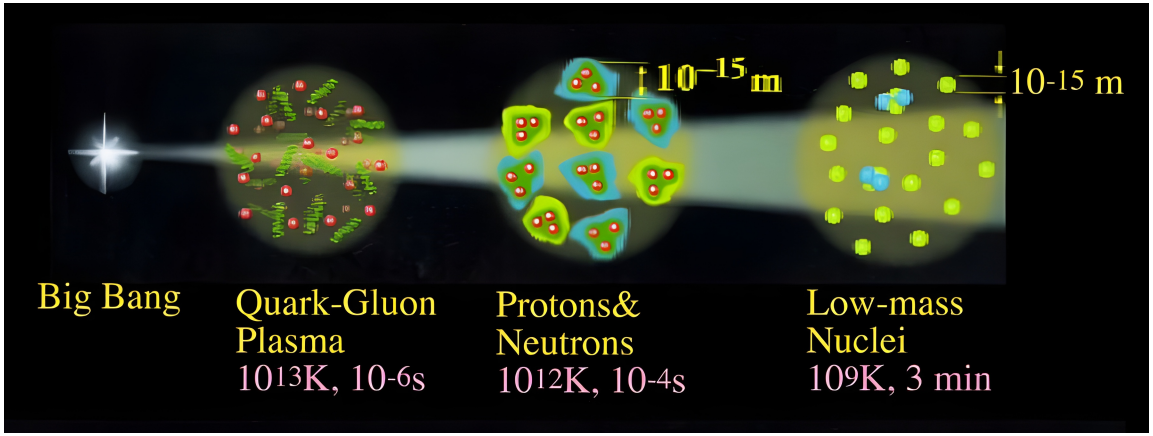


- **After big bang** (few microseconds old) universe is believed to be filled with deconfined state of quarks and gluons

- **Heavy-ion collisions** recreate in the labs, such droplets of matter that filled the universe about $\sim 1 \mu S$ after the big bang

- With heavy-ion collisions we can learn about the properties (Not possible with astronomical) at very **extreme temperature and density** and explore the QCD phase diagram

[4] picture: ncatlab.org;

# Heavy-ion collisions and signatures of QGP

# Evolution of the medium and QGP signatures

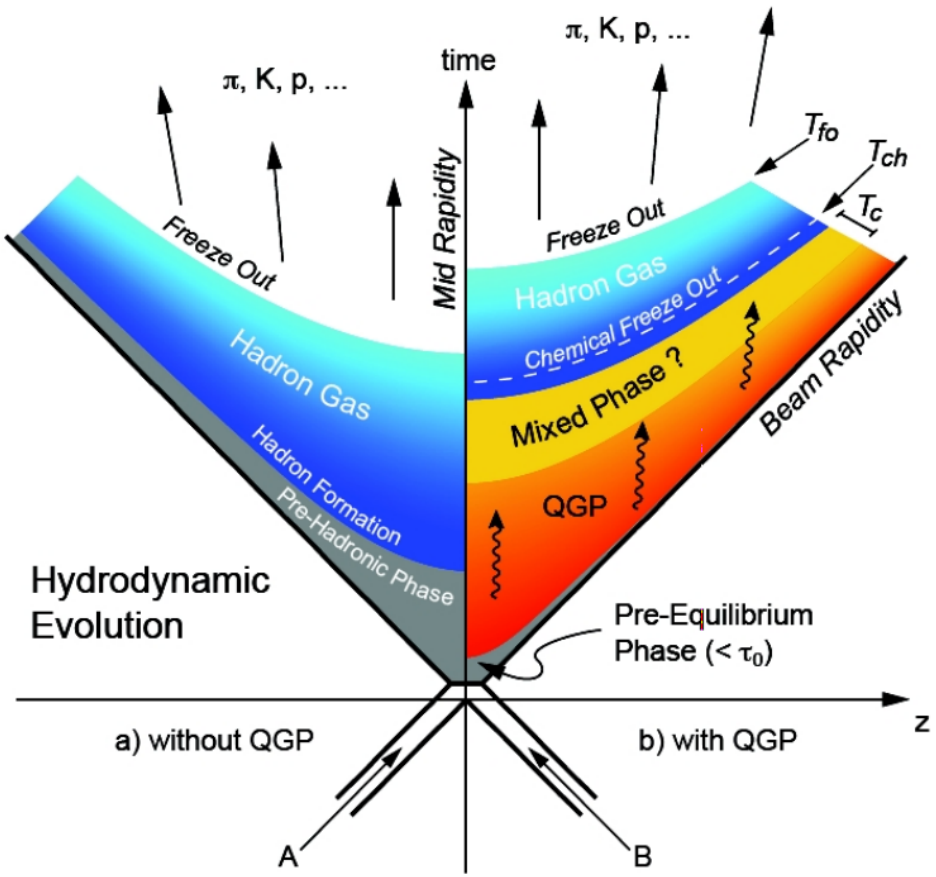


Figure: Evolution of QGP after high energy collisions

## Different ways of probing QGP

- **Jet quenching** (Energy modification of high-$p_T$ jets)
- **Di-lepton production** ($q\bar{q} \rightarrow \mu\bar{\mu}$)
- **Direct photon production** ($q\bar{q} \rightarrow g\gamma$, $qq \rightarrow qq\gamma$ etc.)
- Others: Strangeness enhancement ($q\bar{q} \rightarrow s\bar{s}$, $g\bar{g} \rightarrow s\bar{s}$), Charmonium suppression ($J/\psi$ suppression) etc.

[4] https://particlesandfriends.wordpress.com/2016/10/14/evolution-ofcollisions-and-qgp/

# Source of photons in the different stages of evolution

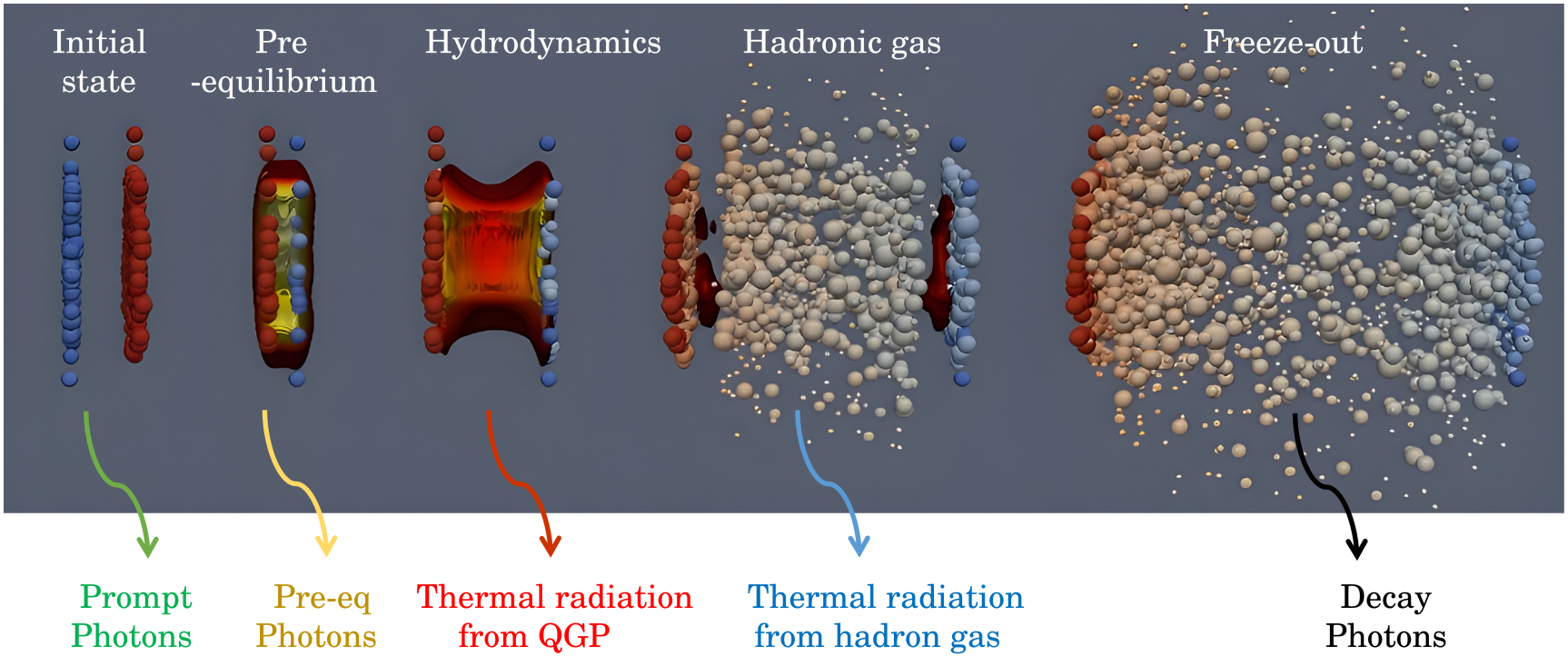


- Photons escape almost **undistorted** after the passage through the strongly interacting environment, allowing access to temperature, flow and density in all regions of the quark-gluon matter and at different moments of the system evolution.

[4] picture: madai colab;

# My research topic: Direct photon study in heavy-ion collisions

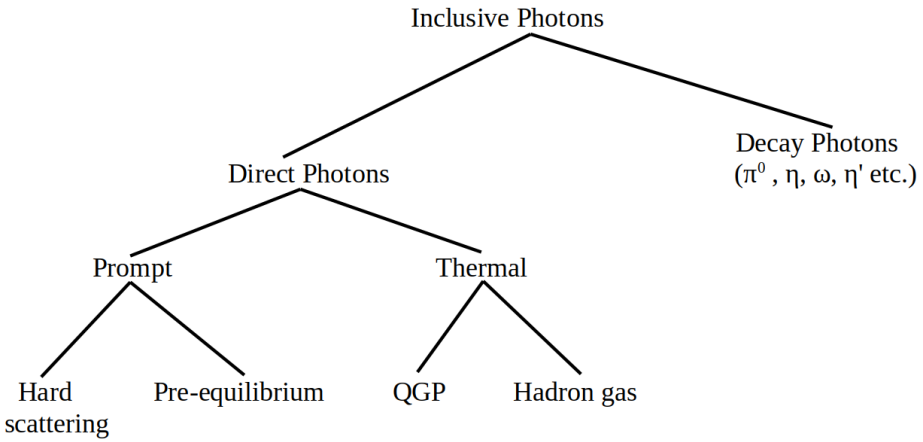


Figure: Photon production in high energy collisions

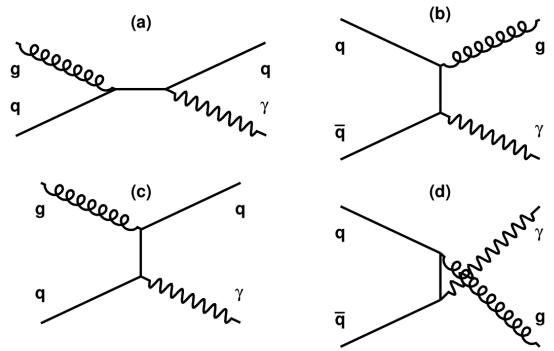


Figure: Prompt photon production in Compton scattering (a and c) and pair annihilation (b and d) processes

- The **prompt photons**(estimated from pQCD acts as standard candle), allows to inspect the *parton distribution functions* and *fragmentation functions* inside the colliding hadrons
- **Thermal photons** are blackbody radiations from thermalized quark-gluon matters(QGP, Hardron gas)
- **Direct photons** are **not** products of the **decay** of the unstable particles($\pi^0$, $\eta$, $\omega$, etc.)

# Experiment: LHC, ALICE, PHOS

# Large Hadron Collider and A Large Ion Collider Experiment (ALICE)


Figure: LHC general view

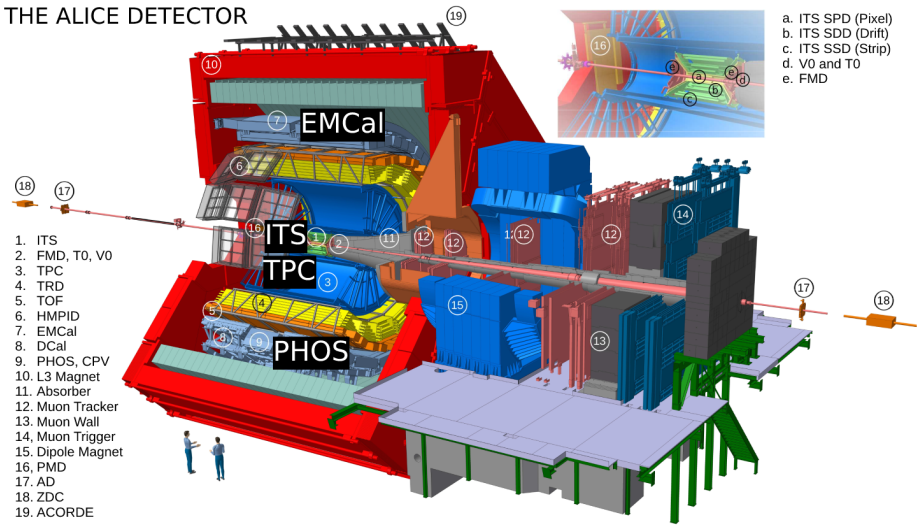


Figure: ALICE detectors during Run2

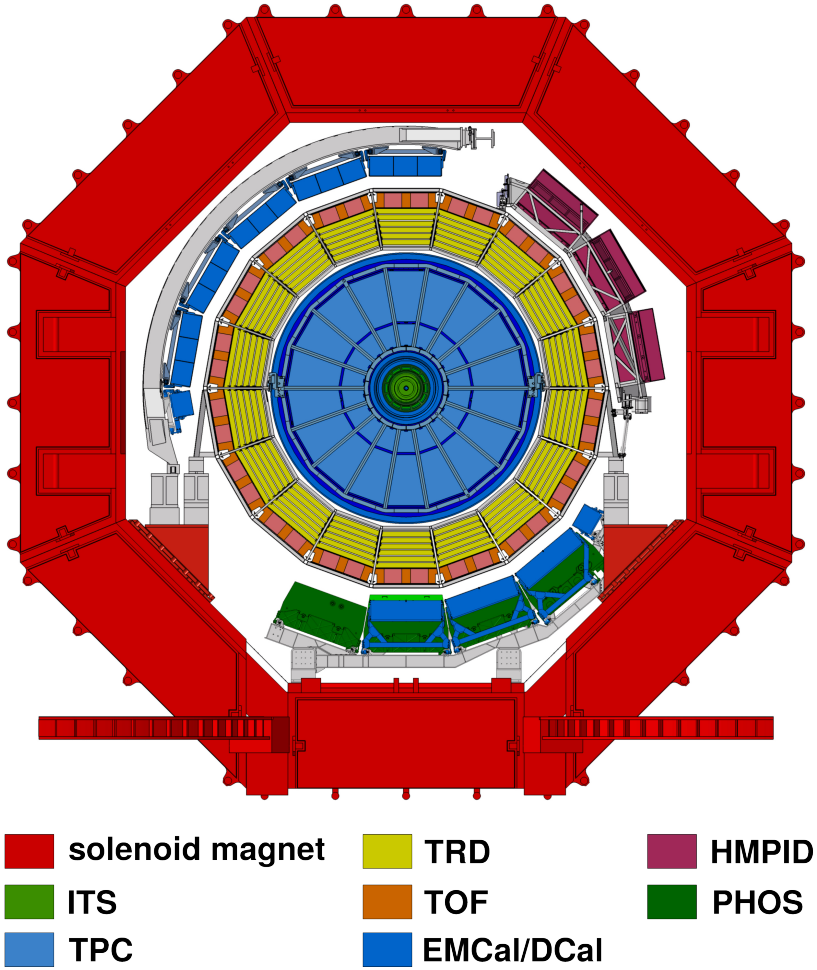


Figure: ALICE cross section view

[1] cern.ch, alice-collaboration.web.cern.ch

# PHOton Spectrometer(PHOS)

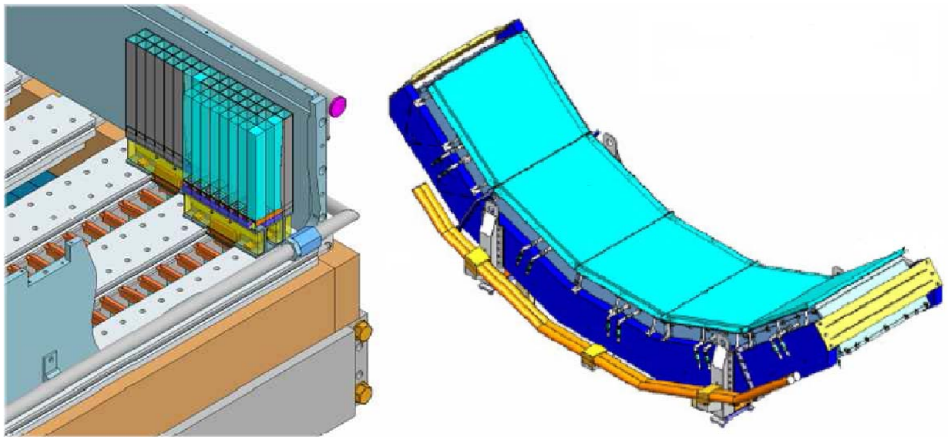

Figure: Photon detetction modules in the ALICE experiment

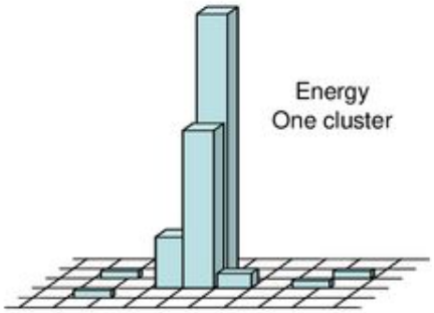


Figure: Cluster formed by energy deposition in the PHOS cells

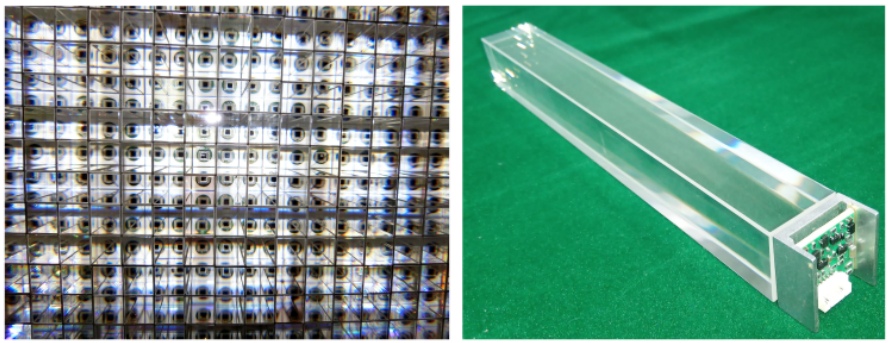

Figure: PHOS cell matrix[left]; A detector element consisting $PbWO_4$ crystal, APD(Avalanche Photo Diode) detector and preamplifier[right]

- Almost 80% of the total cluster energy is deposited in the central cell
- Good at measuring both low energy range and high energy range : 100 MeV to 100 GeV
- At energy range $>$1GeV, the precision is approx. given by $\frac{\sigma_E}{E} = \frac{3\%}{\sqrt{E}} \pm 0.8\%$

[4] alice-collaboration.web.cern.ch

# Collision centrality : $\left(\frac{spectator}{All}\right)$

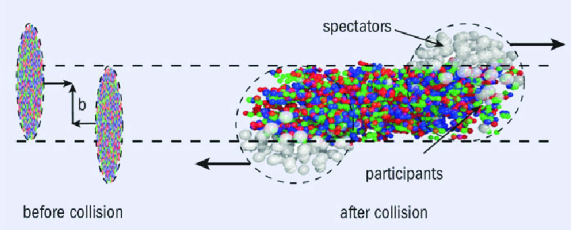


Figure: centrality is the ratio of spectator nucleons to the total no. of nucleons

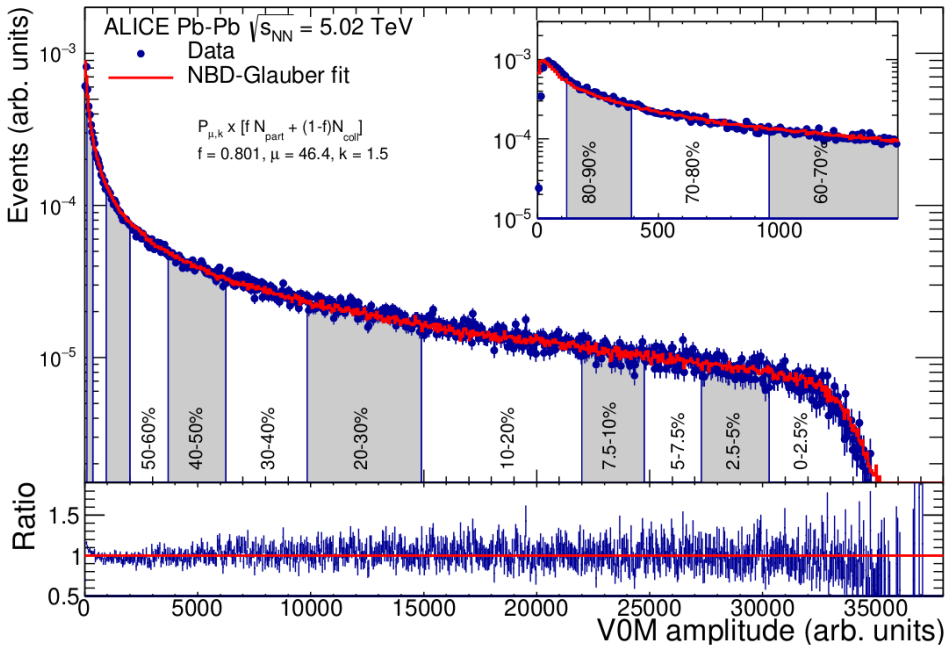


Figure: Distribution of the sum of amplitudes in the V0 scintillators for Pb–Pb collisions at $\sqrt{s_{NN}} = 5.02$ TeV. The distribution is fitted with the NBD-Glauber fit shown as a line. The inset shows a zoom of the most peripheral region.

[4] Centrality determination in heavy ion collisions, ALICE-PUBLIC-2018-011

# Data Analysis: Run2(2016-2018)

# Statistics of the data, events and clusters selection

| Run period | Range of run numbers | Number of selected runs | Total statistics |
|---|---|---|---|
| LHC18r | 296690-297624 | 58 | $41.234 \times 10^6$ |
| LHC18q | 295581-296623 | 131 | $64.970 \times 10^6$ |

Table: Statistics of the data used in our analysis

**Event selection criterion**

- To avoid pile-up of events we impose the following restrictions: **Number of vertex=1**;
- Z-coordinate of the vertex $\leq$10.0 cm.
- To exclude false signals, we choose the **number of contributors** (reconstructed charged particle tracks)$\geq$1.

**Cluster selection criterion**

- minimum energy of **E** $\geq$ **0.3 GeV**
- minimum number of cells **Ncells** $\geq$ **3**
- time of flight of the photons TOF $\leq$ 12.5 ns
- size of the cluster $\geq$ 0.1 cm

# Data quality and calibration of PHOS

# Reconstructing the Invariant mass of $\pi^0$ meson from two photons decay

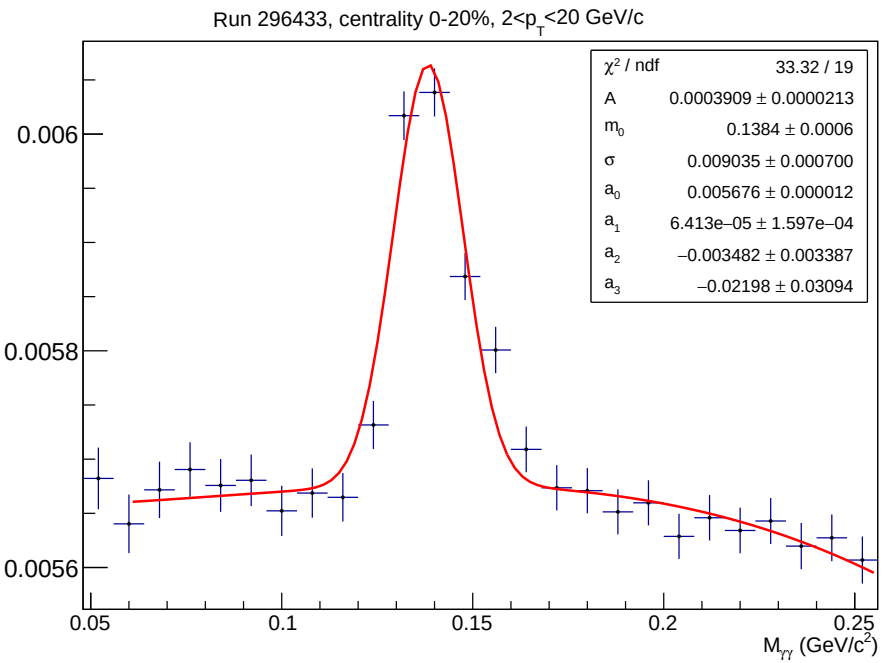


Figure: Invariant mass of $\pi^0$ in a particular run(296433) in a given centrality(00-20%) by fitting the signal with gaussian and the combinatorial background by 3rd order polynomial

- $\pi^0 \rightarrow \gamma + \gamma$ (BR : 98.8%)
- Invariant mass of two photons, $M_{\gamma\gamma} = \sqrt{2E_{\gamma_1}E_{\gamma_2}(1-\cos\theta)}$
- Signal (Gaussian) : $A \cdot \exp\left[-\frac{(m-m_0)^2}{2\sigma^2}\right]$
- Background (3rd order polynomial) : $a_0 + a_1(m-m_0) + a_2(m-m_0)^2 + a_3(m-m_0)^3$

# Data quality assurance: Run-by-run study of $\pi^0$ peak position

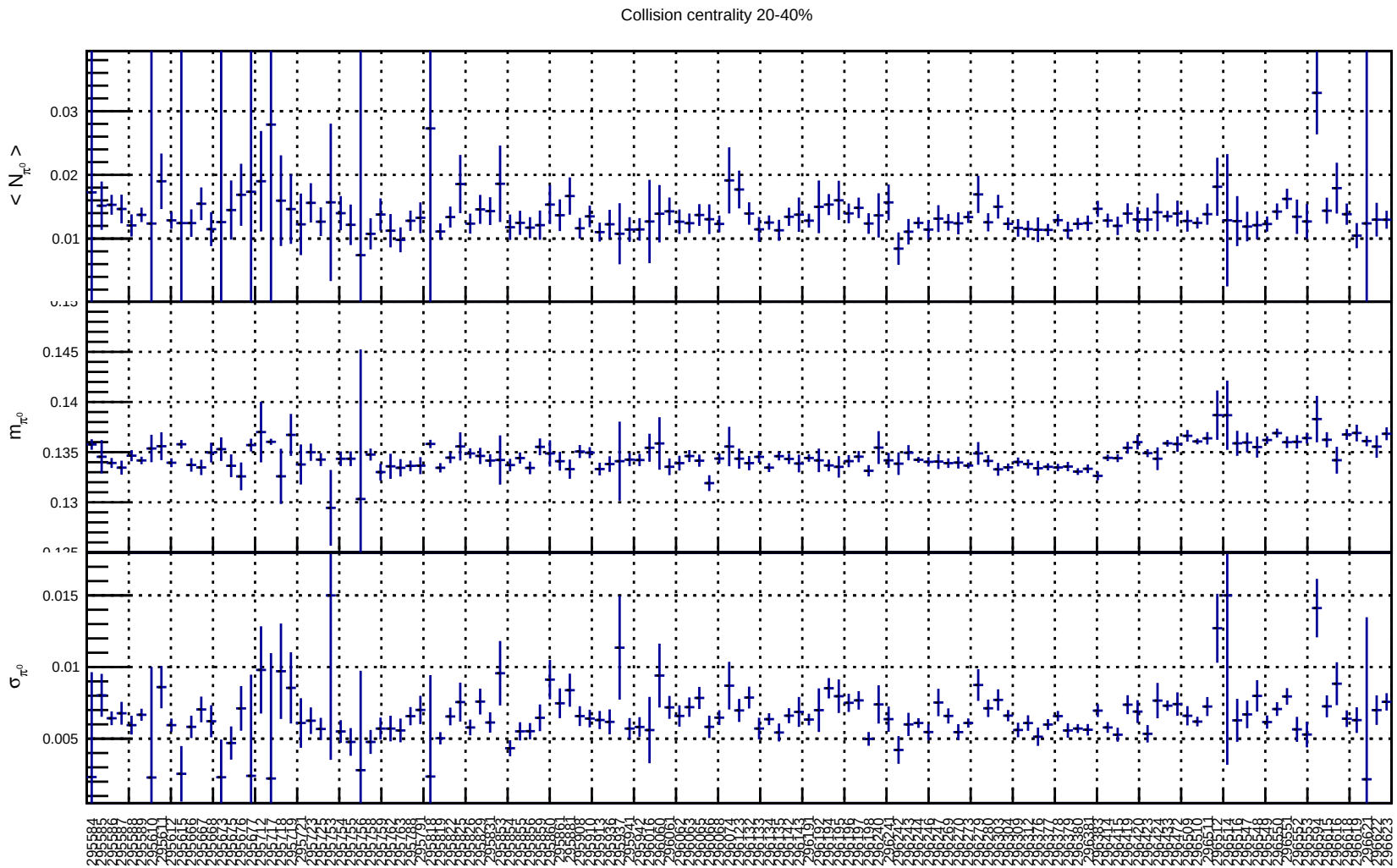


Figure: The run numbers corresponding to the run period LHC18q is given in the x-axis

# E/p ratio of measurements for electrons(and positrons)

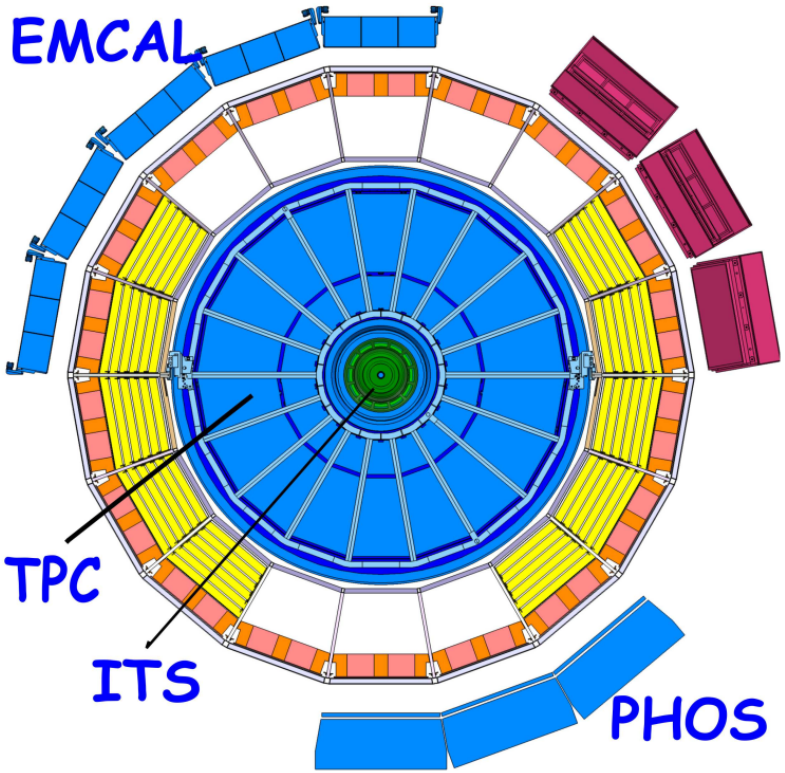


Figure: Independent measurements of momenta (in ITS and TPC) and energy (in PHOS) of electrons(and positrons)

- $E = \sqrt{(p^2 + m_e^2)}$
- $m_e = 0.0005 GeV << p(\sim GeV)$
- E ≈ p or, E/p ≈ 1
- 'p' is measured by ITS and TPC using curvature of the trajectory whereas 'E' is measured in PHOS

# Calibration of PHOS: E/p ratio of beta particles in run period LHC18r

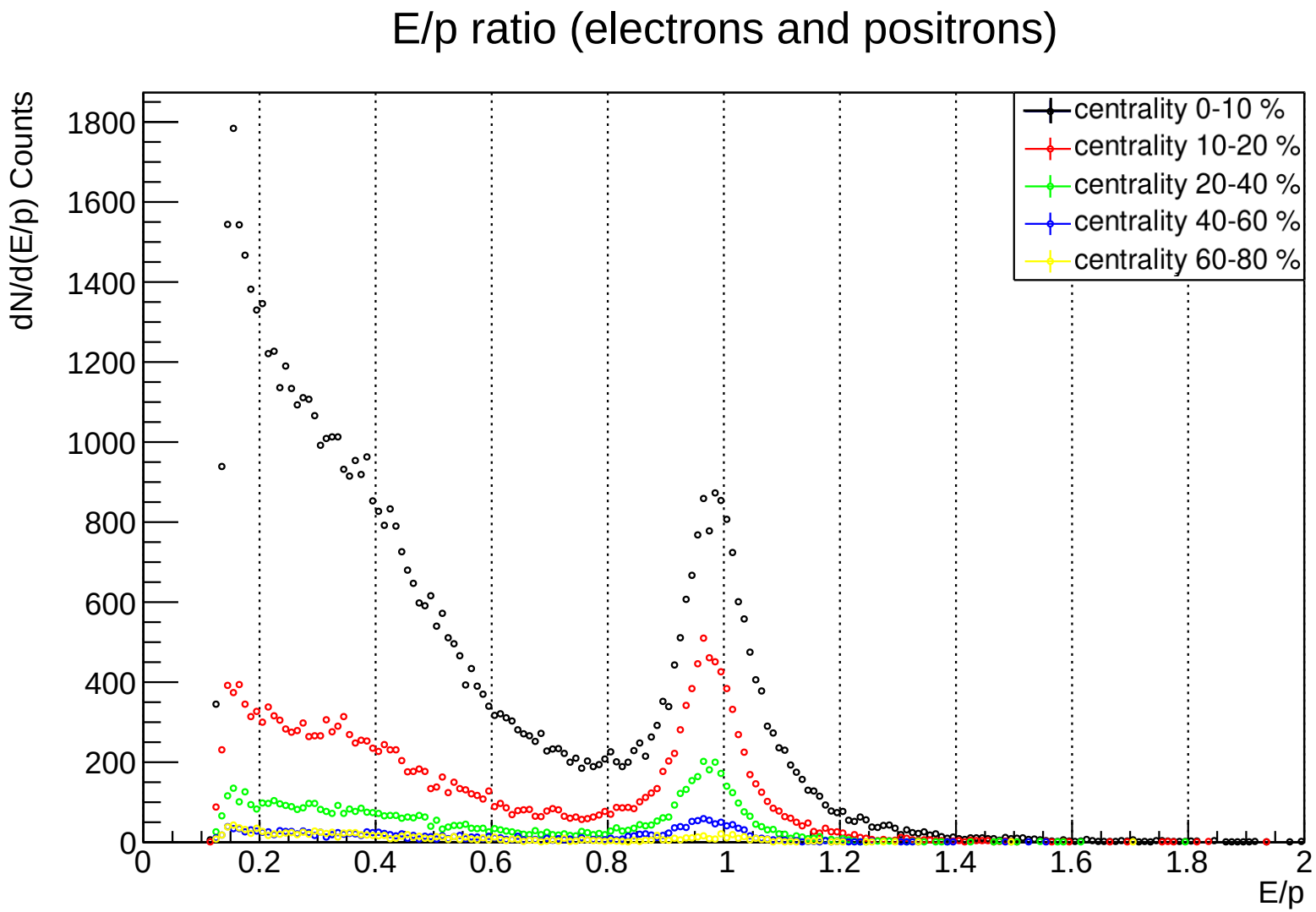


Figure: Differential count vs E/p ratio of electrons

# Inclusive photons from the raw yield of clusters

# Reconstruction of the photon spectrum with PHOS:Inclusive photons($\gamma^{inc}$)

Invariant yield of photons is found as

$$E\frac{d^3N_{\gamma^{inc}}}{dp^3} = P_\gamma \times \frac{1}{\epsilon_\gamma} \times \left(\frac{1}{N_{\text{ev}}} \times \frac{1}{2\pi} \times \frac{1}{p_{\text{T}}}\frac{d^2N_{PHOS}}{dp_{\text{T}}dy}\right) \tag{1}$$

$N_{PHOS}$ - number of photons reconstructed in PHOS.

$N_{ev}$ - number of analyzed events.

$P_\gamma$ - purity of the photon sample, number of PHOS photons produced by $\gamma$ particles divided by the number of all PHOS photons

$$P_\gamma = \frac{N_{\gamma\ PHOS}}{N_{PHOS}} \tag{2}$$

$\epsilon_\gamma$ - efficiency of the $\gamma$ detection, ratio of $\gamma$ clusters in PHOS to the number of $\gamma$-s produced in the collisions:

$$\epsilon_\gamma = \frac{N_{\gamma\ PHOS}}{N_{\gamma\ All}} \tag{3}$$

# Raw yield of clusters in PHOS for LHC18r (different centralities)

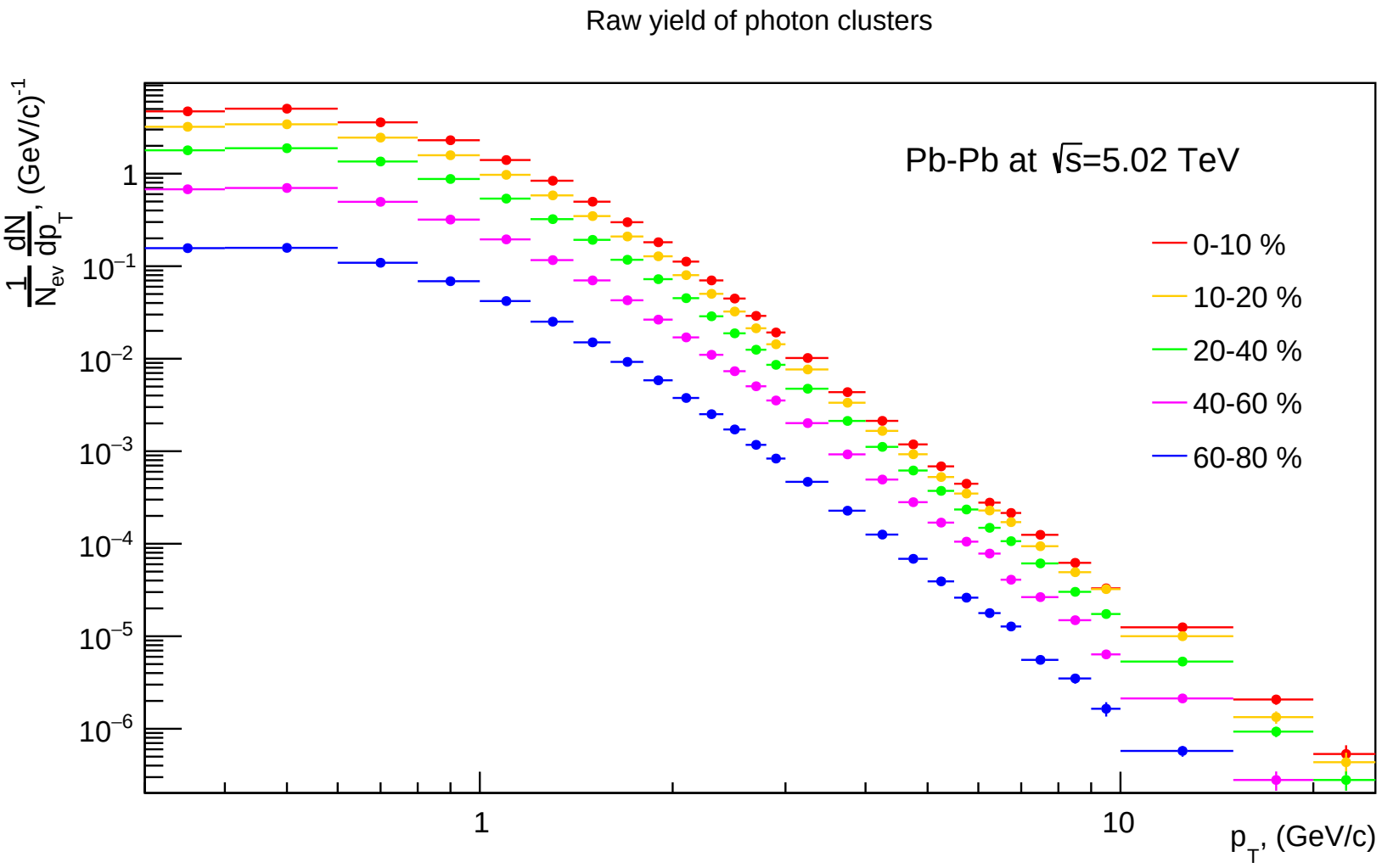

# Purity of Photon cluster samples

# Contamination in the photon samples

$$N_{cluster} = N_{\gamma} + N_{e^{\pm}} + N_{\pi^{\pm}} + N_{K^{\pm}} + N_{p} + N_{\bar{p}} + N_{n} + N_{\bar{n}} + N_{K^{0}_{L}} + N_{K^{0}_{S}} + .....$$

- Using **MC data** we can simulate the clusters due to other particles
- **CPV cut:** The clusters are removed if they are too close to the charged tracks($e^{\pm}, \pi^{\pm}, K^{\pm}, p$) measured by CPV [and ITS detector]
- **Dispersion cut:** Based on cluster characteristics (e.g. shower shape) we minimize contaminations of other particles including neutral particles

The ionization loss in $PbWO_4$ for $\mu^{\pm}$ is very small compared to energy cut($< 0.3$ GeV) for event selection

# PHOS sample purity using vertex photons

$$Purity(p_T) = \frac{N_{\gamma_{clusters}}(p_T)}{N_{all_{clusters}}(p_T)}$$

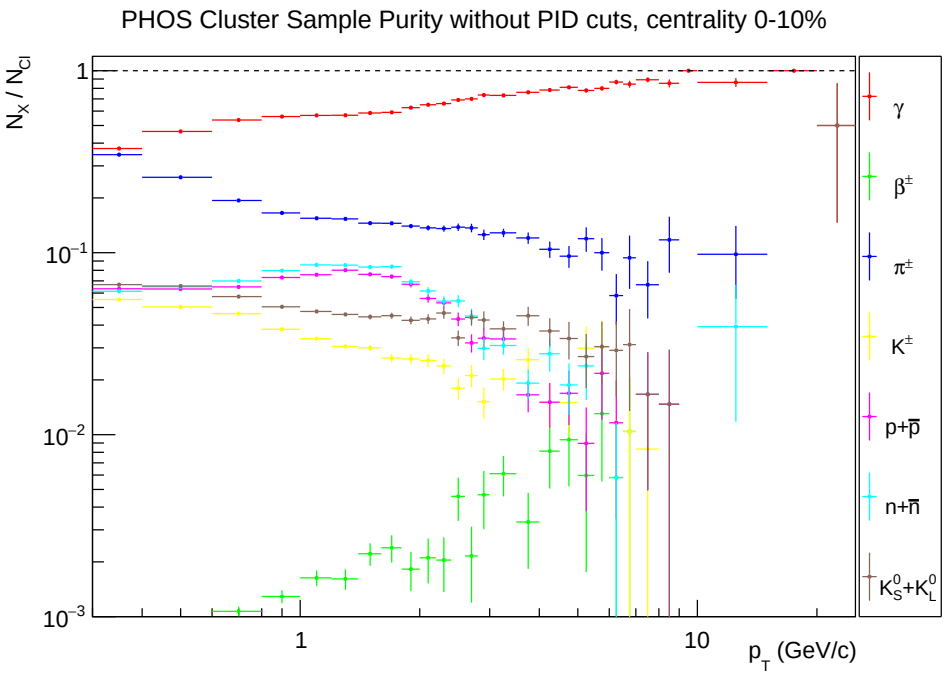


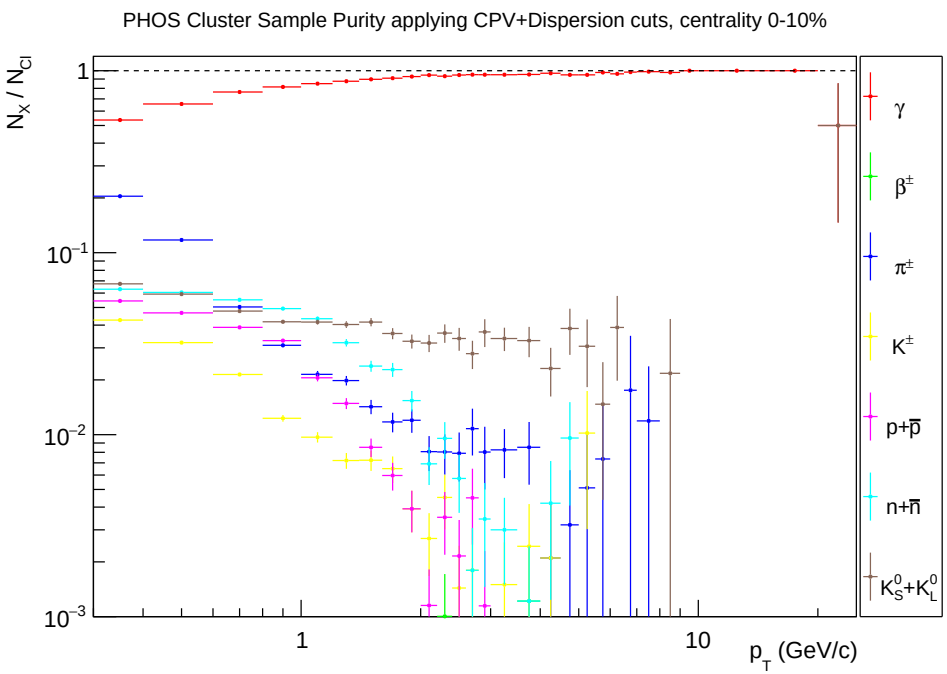

# Efficiency of PHOS

# Efficiency of photon detection in PHOS

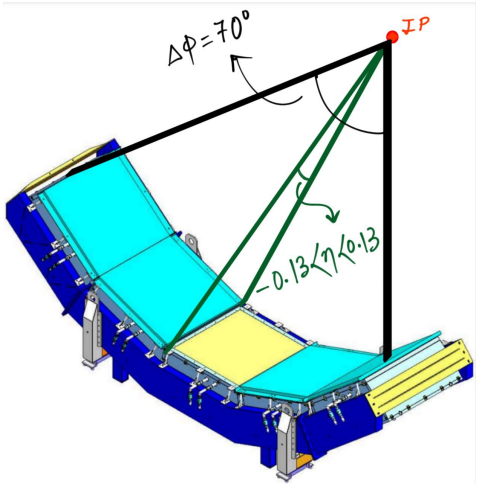


Figure: Modules of the PHOS detector and its angular coverage

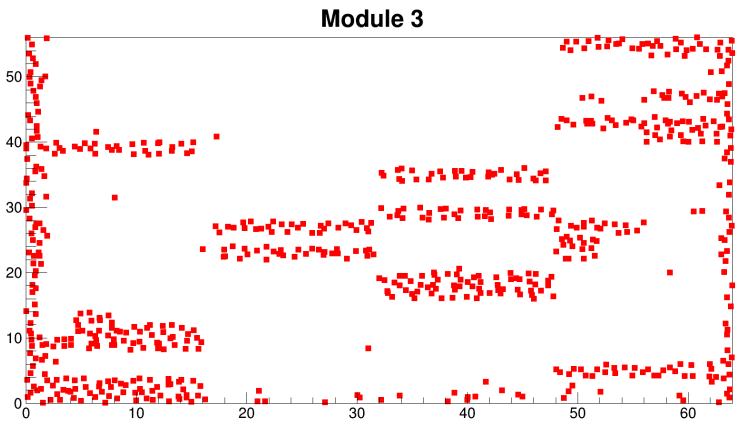


Figure: Red squares represent Bad channels, LHC18r Module3

- For photons emitted at mid-rapidity, $|y| < 0.5$, $0 < \phi < 2\pi$, only **5.1% of all photons** fly into the PHOS solid angle
- Photons can be caught inside **bad electronic** channel
- Converted into **electron-positron** pair, which is **deflected** by magnetic field
- Entirely **absorbed** or dispersed by material of **tracking detector**
- Photons may impinge on calorimeter surface **close to a charged particle**
- Sometimes, photons may create **shower similar to a hadron** and be discarded

# Efficiency for different centralities (applying CPV+Dispersion cut)

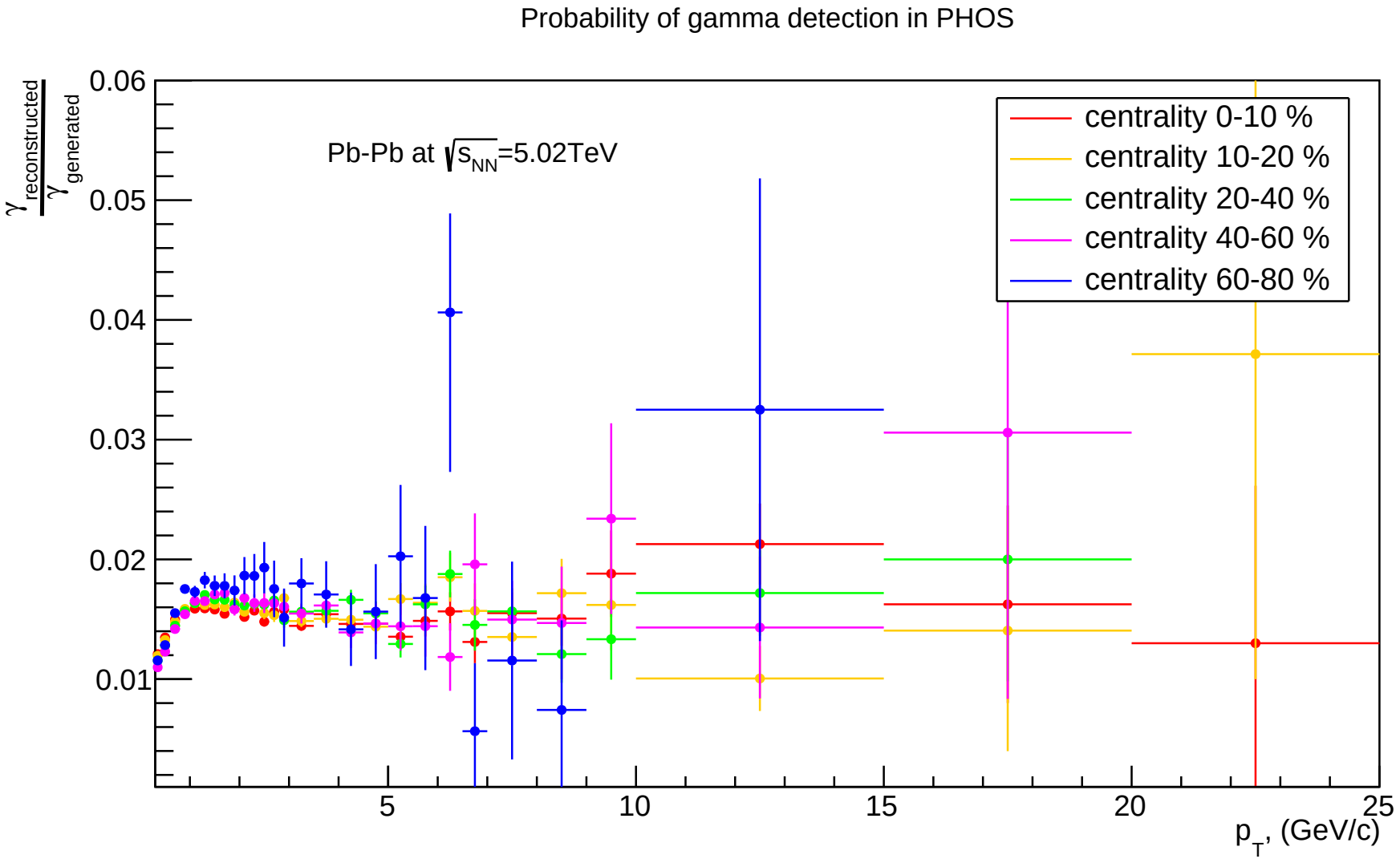

# Invariant yield of inclusive photons : Different centralities

$$P_\gamma \times \frac{1}{\epsilon_\gamma} \times \left( \frac{1}{N_{\text{ev}}} \times \frac{1}{2\pi} \times \frac{1}{p_{\text{T}}} \frac{d^2 N_{PHOS}}{dp_{\text{T}} dy} \right) \tag{4}$$

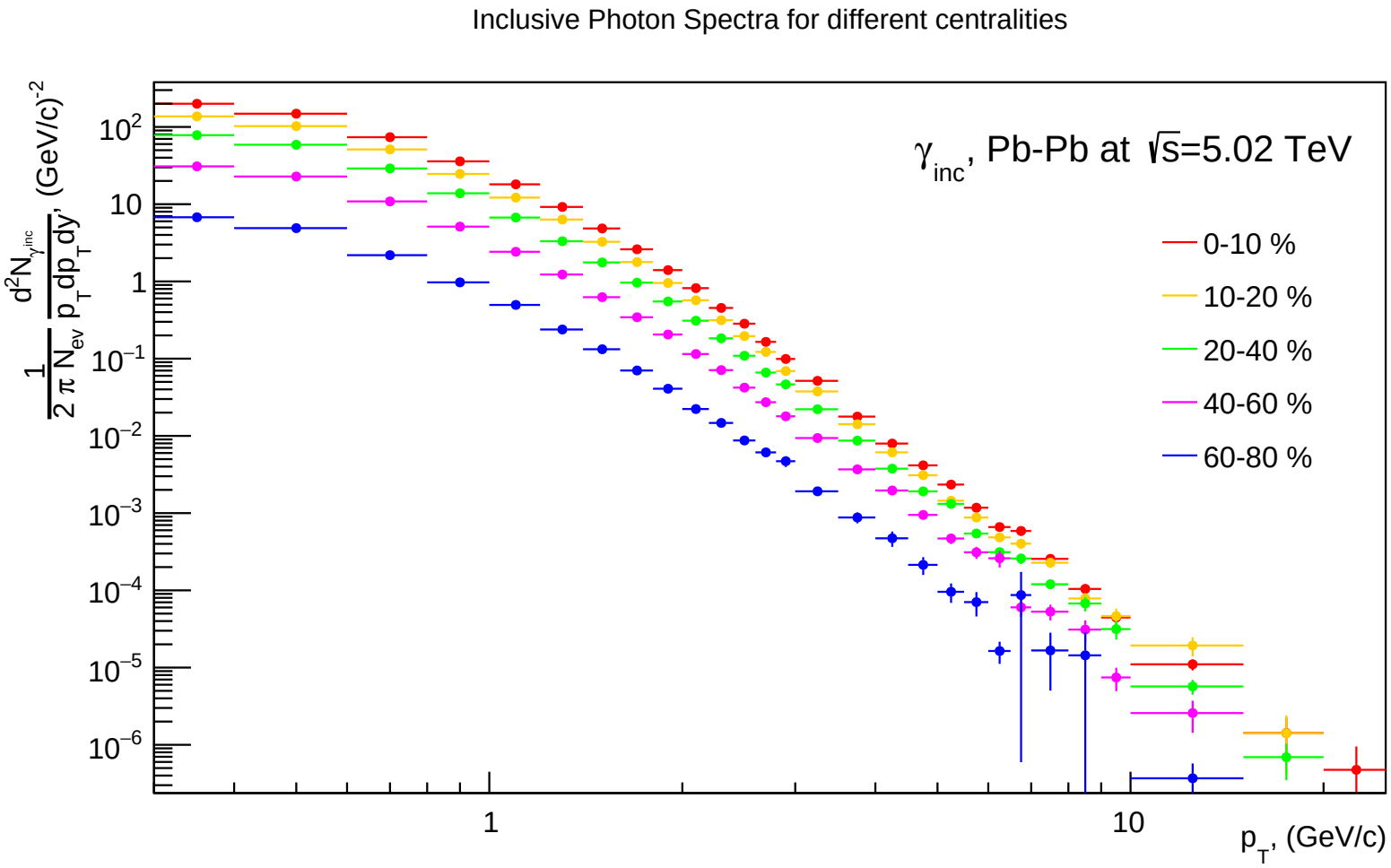

# Simulation of the decay photon background

# Background photon estimation using MC cocktail generation

| Particle | Mass (MeV/$c^2$) | Decay channel | Branching ratio (%) |
|---|---|---|---|
| $\pi^0$ | 135 | $\gamma\gamma$ | 98.8 |
| | | $\gamma e^+ e^-$ | 1.2 |
| $\eta$ | 547 | $\gamma\gamma$ | 39.2 |
| | | $\gamma\pi^+\pi^-$ | 4.8 |
| | | $\gamma e^+ e^-$ | $4.9 \times 10^{-3}$ |
| $\omega$ | 782 | $\pi^0\gamma$ | 8.3 |
| | | $\eta\gamma$ | $4.6 \times 10^{-4}$ |
| $\eta'$ | 958 | $\rho^0\gamma$ | 29.1 |
| | | $\omega\gamma$ | 2.8 |

Table: Particles decaying into photons

- **Hagedorn function** [5]: $\frac{d^2N}{dydp_T} = p_T \cdot A\left(\exp(ap_T + bp_T^2) + \frac{p_T}{p_0}\right)^{-n}$
  This functional form approaches an exponential at low $p_T$ and a power law at larger transverse momenta and describes the measured spectra over full measured range
- **Transverse mass scaling :** $m_T = \sqrt{p_T^2 + m_0^2}$; $\frac{d^2N}{p_T dp_T dy} = \frac{d^2N}{m_T dm_T dy}$
  Transverse momenta spectra,
  $f_X(p_T, X) = C \times \frac{p_{T,X}}{\sqrt{m_{0,x}^2 + p_{T,x}^2 - m_{0,R}^2}} \times f_R(\sqrt{m_{0,x}^2 + p_{T,x}^2 - m_{0,R}^2})$

[5] Centrality determination in heavy ion collisions, ALICE Collaboration, 2018

# Hadronic decay photon spectra using MC cocktail simulation

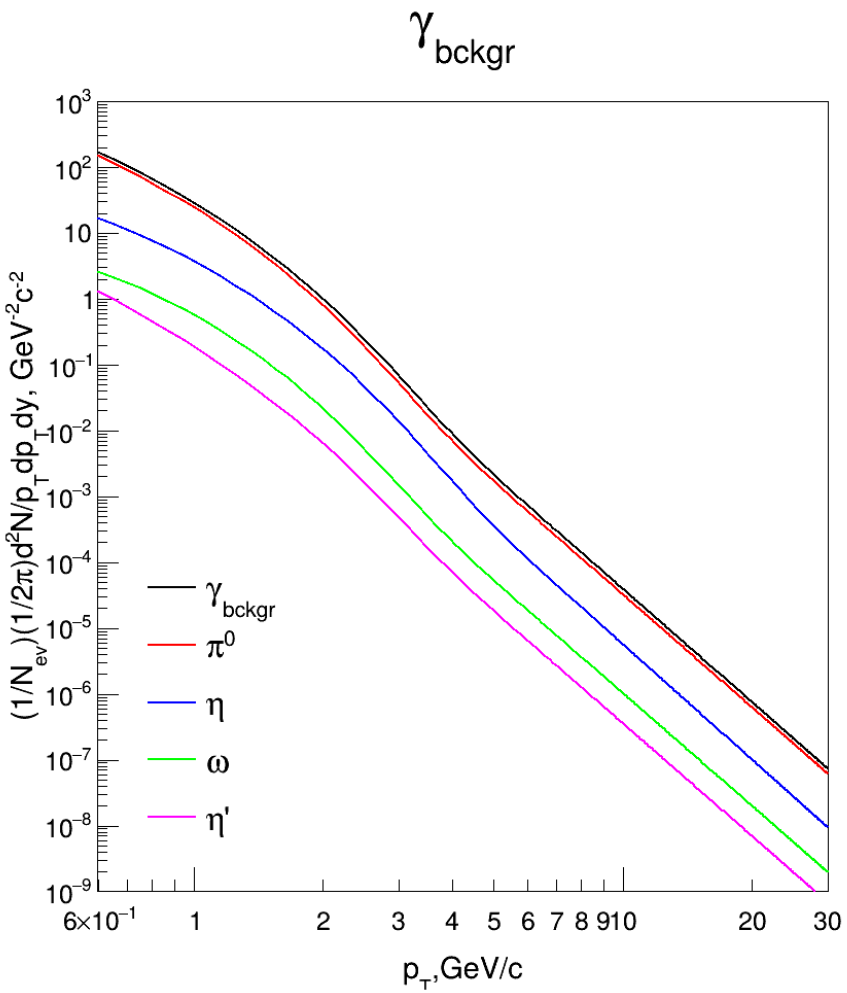


Figure: Shape of input hadrons and background photons

- $\pi^0$ and $\eta$ mesons are generated using parametrization. $\omega$ and $\eta'$ are generated using transverse mass scaling of $\pi^0$ spectra

# Decay photon cocktail in Pb–Pb collisions at $\sqrt{s_{NN}} = 5.02$ TeV centrality 0-10 %

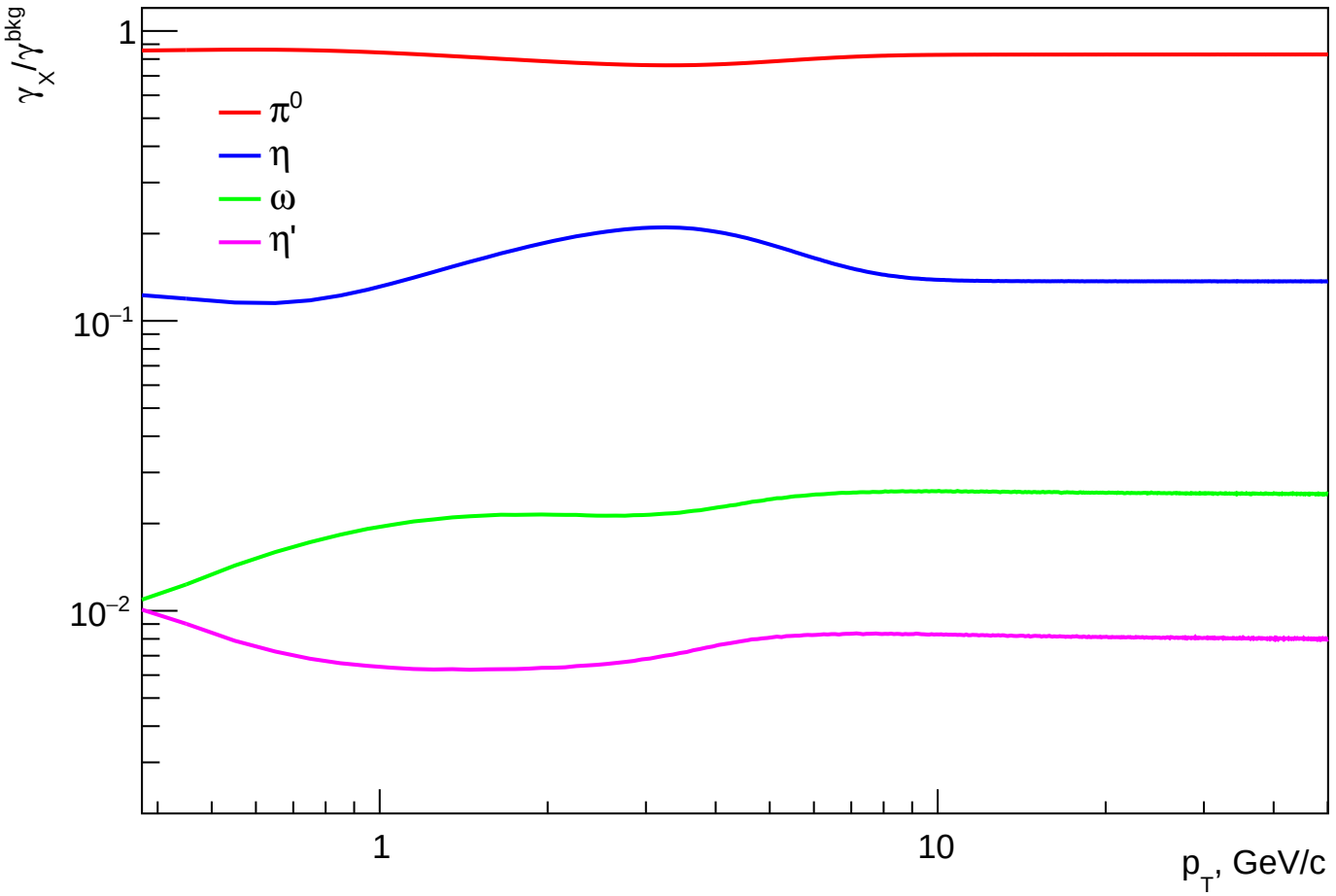


Figure: Fraction of various hadronic decay sources [$\pi^0$ ($\sim$ 90%) is the most dominant background]

# Inclusive and decay photon spectra for centrality 0-10 %

compared with pertubative-QCD results (for different factorization scales)

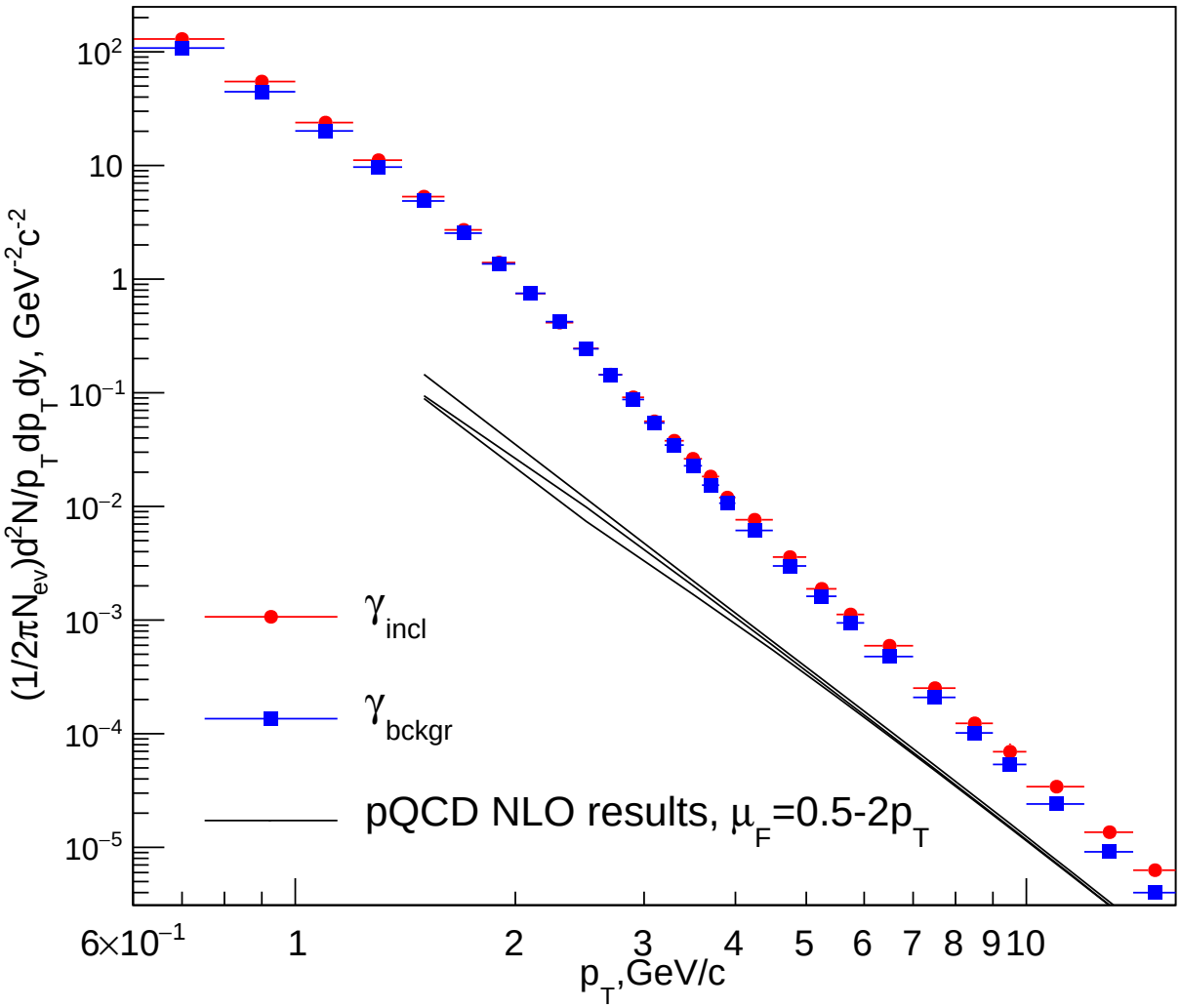

# Direct photons using the Double ratio

# Direct photons($\gamma_{\text{direct}}$) spectra using the Double ratio($R_D$)

$$R_\gamma = \frac{\gamma^{\text{inc}}}{\gamma^{\text{decay}}} \approx \left(\frac{\gamma^{\text{inc}}}{\pi^0_{\text{meas}}}\right)_{\text{data}} \Big/ \left(\frac{\gamma^{\text{decay}}}{\pi^0_{\text{param}}}\right)_{\text{MC}} = R_D \tag{5}$$

$$\gamma_{\text{direct}} = \gamma_{\text{incl}} - \gamma_{\text{decay}} = \left(1 - \frac{1}{R_D}\right) \gamma_{\text{incl}} \tag{6}$$

Finally, the direct photons invariant yield can be calculated as follows,

$$\frac{1}{2\pi N_{\text{ev}}} \frac{d^2 N_{\gamma\, dir}}{p_{\text{T}} dp_{\text{T}} dy} = \frac{1}{2\pi N_{\text{ev}}} \frac{d^2 N_{\gamma\, inc}}{p_{\text{T}} dp_{\text{T}} dy} \left(1 - \frac{1}{R_D}\right) \tag{7}$$

# $\gamma/\pi^0$ ratios for the calculation of the double ratio($R_D$)

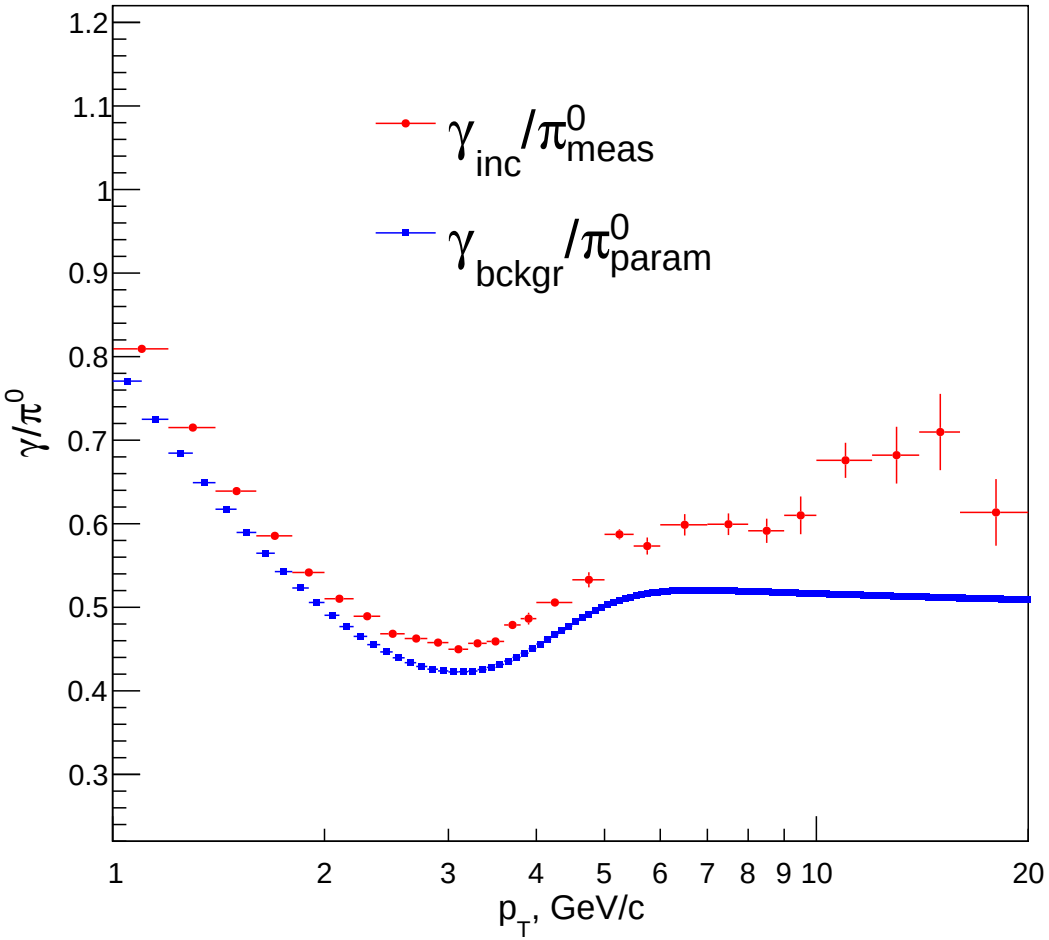


Figure: The photons transverse momentum dependence of $\gamma/\pi^0$ ratios from the experiment and Monte-Carlo cocktail simulation

# Double ratio for Pb-Pb at $\sqrt{s} = 5.02$ TeV, centrality 0-10%

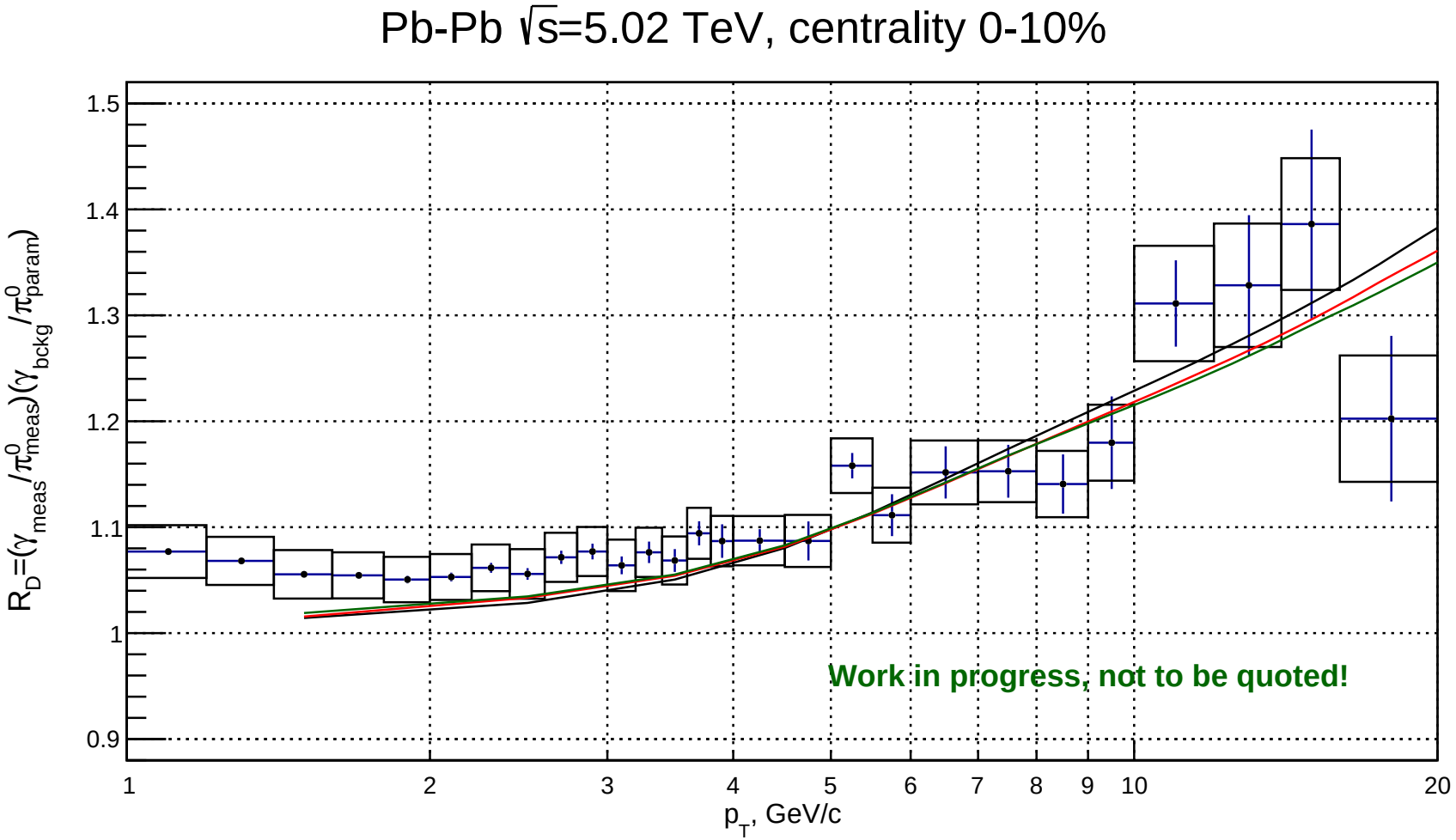


Figure: Double ratio for centrality 0-10 % with statistical (error bars) and systematic (rectangles) errors. Black, red and green curves refer to the NLO pQCD predictions for factorization scales $\mu_F = 0.5, 1, 2p_T$, respectively.

# Invariant yield of direct photons and temperature estimation

# Direct photon invariant yield and estimation of the effective temperature

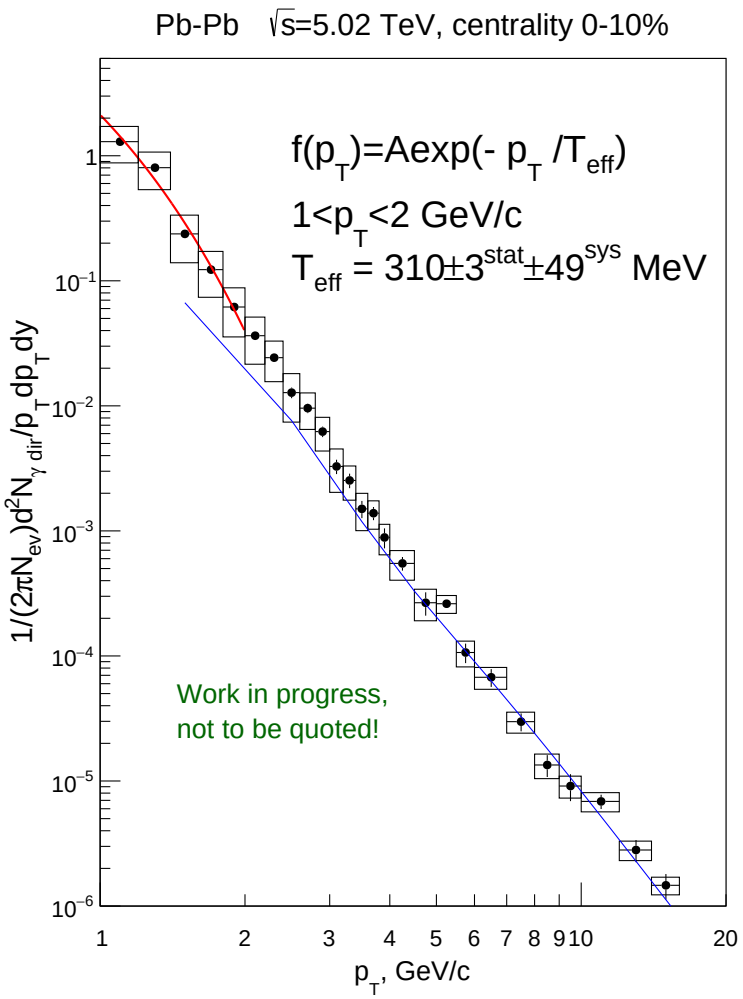


Figure: Invariant yield of direct photons compared against NLO pQCD predictions

The invariant yield of direct photons demonstrates an **excess over the pQCD prediction**, which may indicate a presence of thermal photons.

We fit the invariant yield of the direct photons with an exponential function in the interval $1 < p_T < 2$ GeV/c

The effective temperature is the inverse slope of the exponent: $T_{\text{eff}} = 310 \pm 3^{\text{stat}} \pm 49^{\text{sys}}$ MeV.

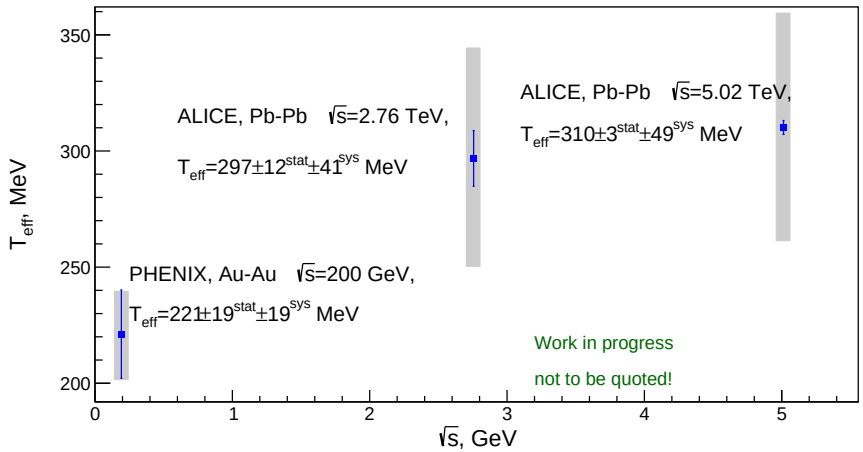


Figure: Results for the effective temperature from different heavy ion experiments and collision energies.

# Fitting the difference between the measured direct photon invariant yield and the pQCD NLD predictions

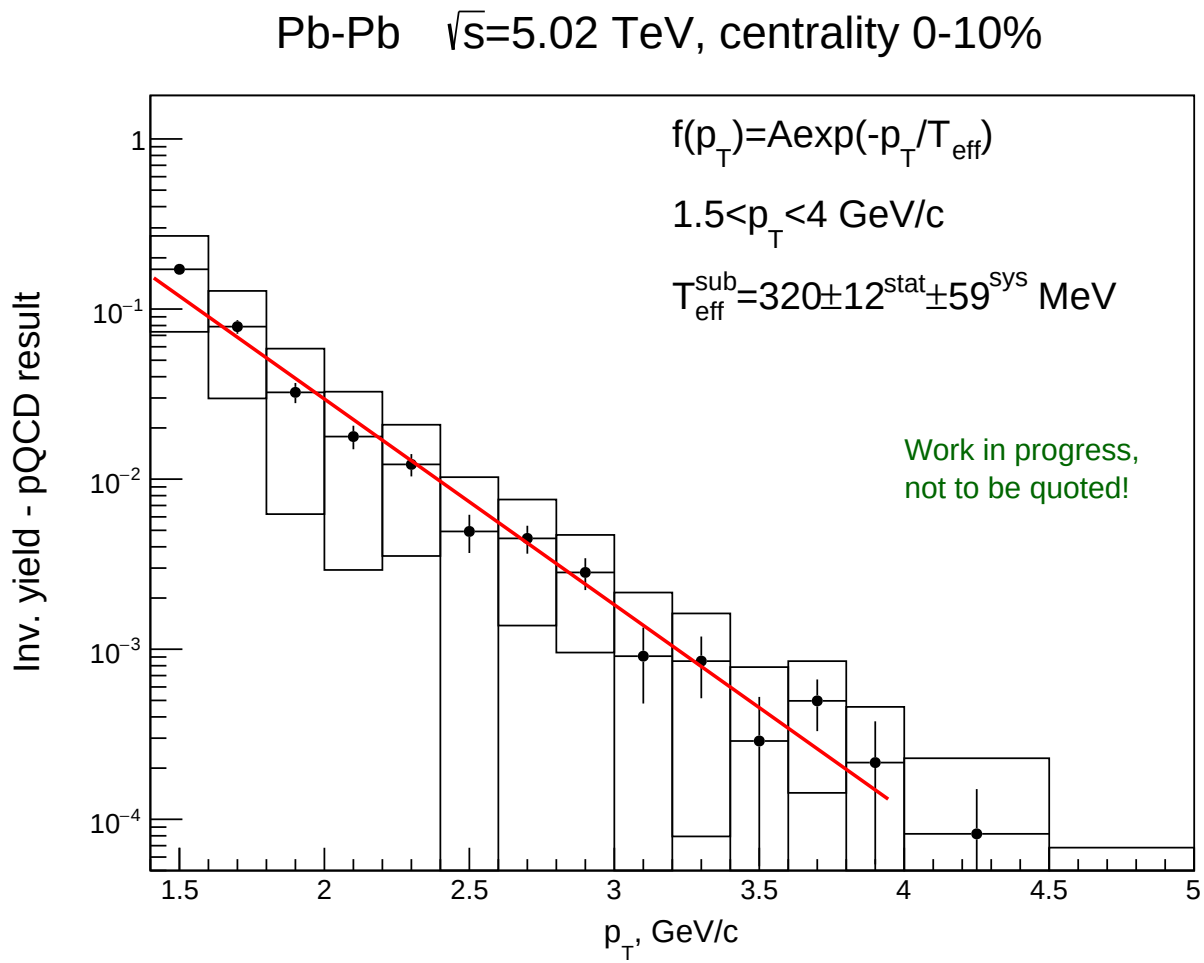


Figure: Thermal photons in low pT(1.5 GeV) to 4 geV where pQCD results are available to estimate the average temperature of the medium

# Last topic: Anisotropic flow

# Anisotropic Flow

Asymmetry in the initial geometry → anisotropy in particle momenta distributions

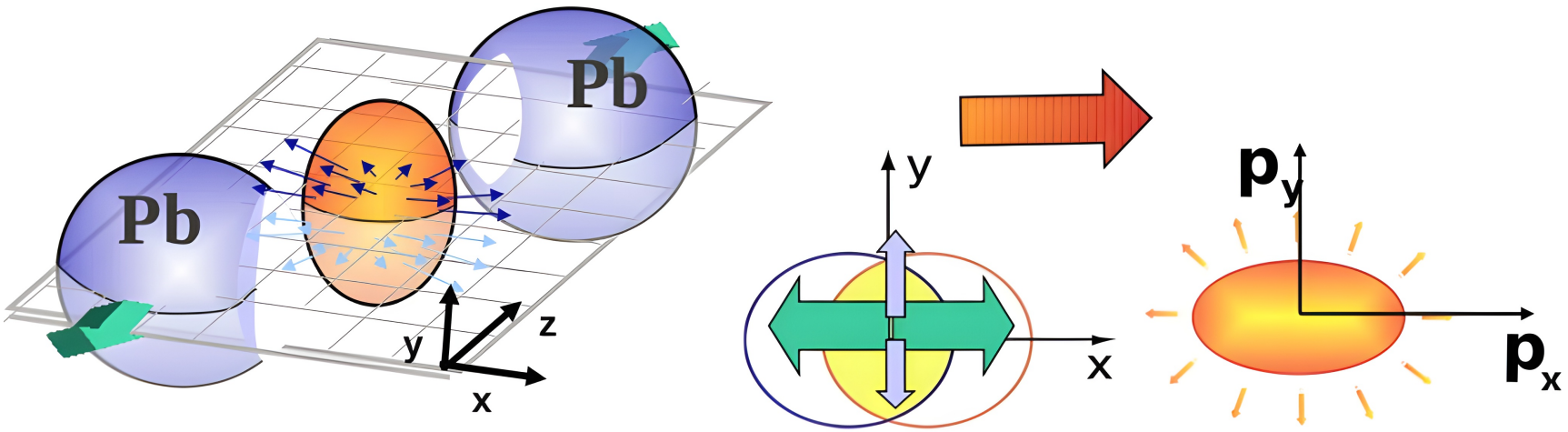


**Azimuthal anisotropy can be described by Fourier expansion of particles' angular distribution around the beam direction:**

$$E\frac{d^3N}{d^3\mathbf{p}} = \frac{1}{2\pi p_t}\frac{d^2N}{dp_t dy}\left(1 + 2\sum_{n=1}^{\infty} v_n \cos\left[n(\varphi - \Psi_{\mathrm{RP}})\right]\right) \tag{8}$$

where, $v_1$ (Directed flow), $v_2$ (Elliptic flow), $v_3$ (Triangular flow), ... are the Fourier coefficients.

# Elliptic Flow of direct photons

$$v_{2,\mathrm{dir}} = \frac{R_\gamma v_{2,\mathrm{inc}} - v_{2,\mathrm{decay}}}{R_\gamma - 1} \tag{9}$$

where $R_\gamma$ is the photon excess ratio, $v_{2,\mathrm{inc}}$ represents the inclusive flow, and $v_{2,\mathrm{decay}}$ is the decay photon flow.

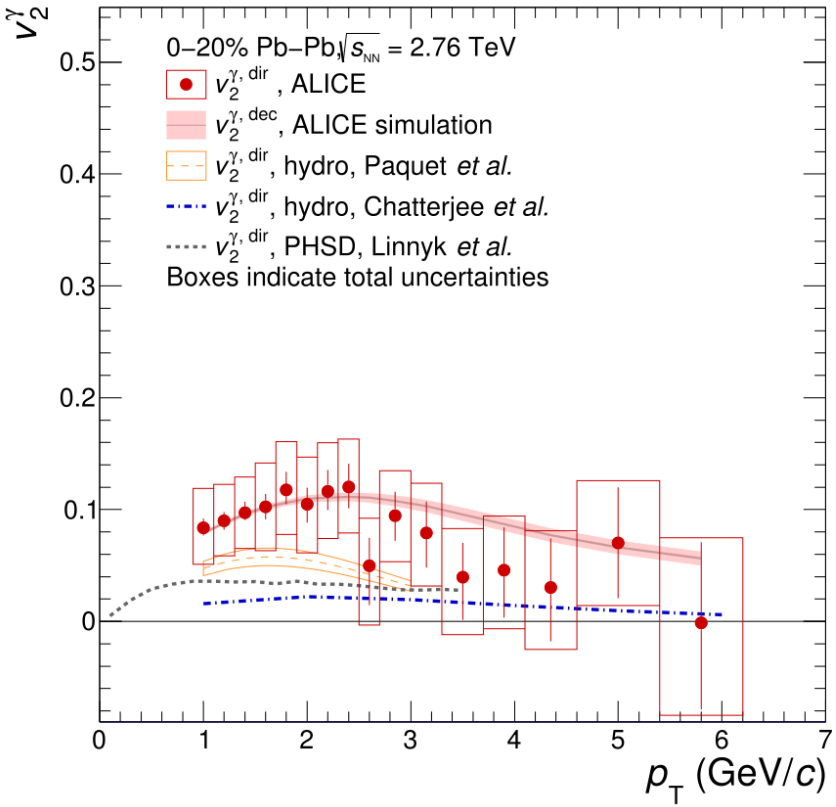


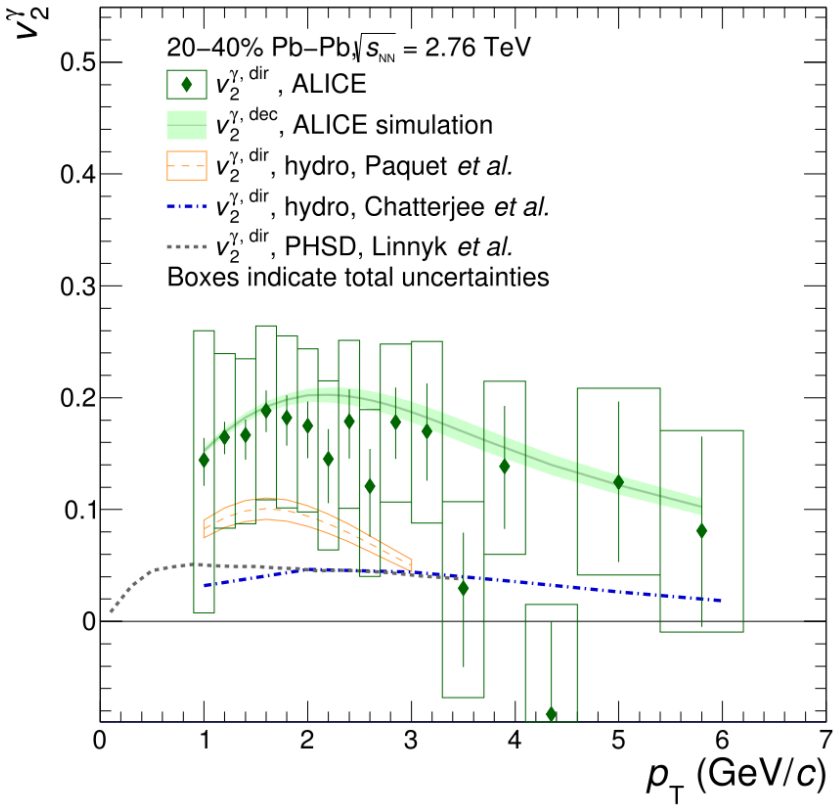


6

[6] Figure reference: *Physics Letters B 789 (2019) 308–322*

# Summary

- In extreme conditions, the hadronic matter enters into deconfined state of quark-gluon matter
- In Heavy-ion collisions(e.g. ALICE, PHENIX) QCD and phase transitions are studied
- Photons act as unique probe to study the quark-gluon matter at various stages
- Temperature and flow can be studied from direct photon spectra, giving us information about various stages of the evolution

THANK YOU FOR LISTENING!

# BACKUP SLIDES

# Direct Photon Puzzle

- Large direct photon yields and significant elliptic flow
- Contradiction between large photon yields (expected at early stages) and large anisotropy (expected at late stages).
- Theoretical models struggle to explain both yields and anisotropy simultaneously
- The ”direct photon puzzle” has inspired extensive theoretical work and new models

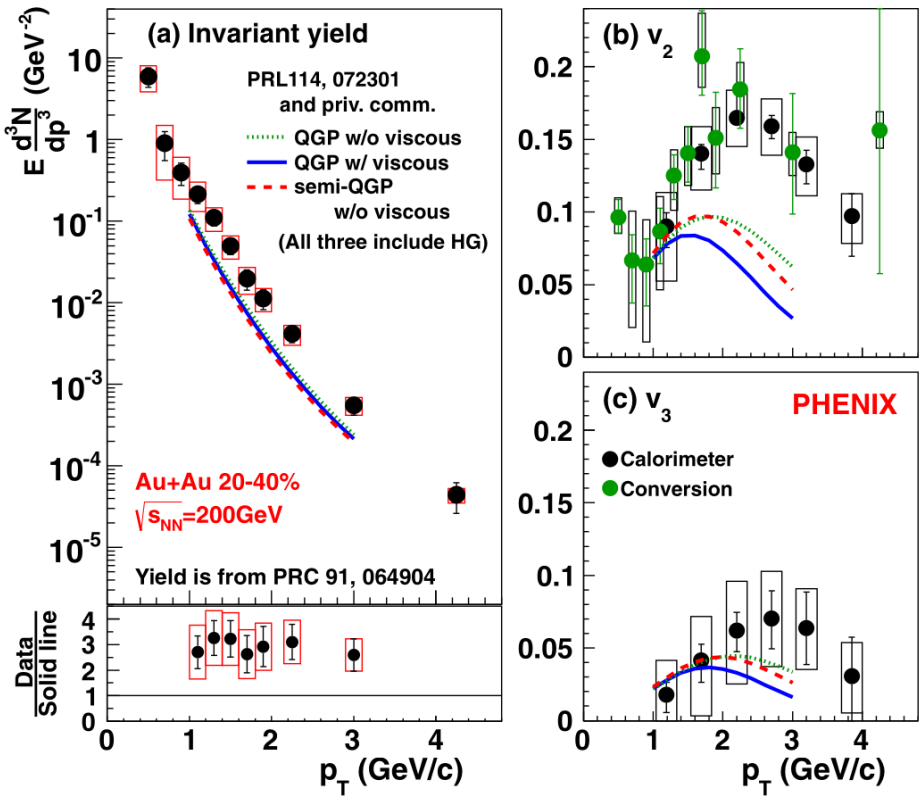


*PHYSICAL REVIEW C 94, 064901 (2016)*

# Double Ratio : To reduce systematic uncertainty

$$\text{Decay 1: } X \rightarrow A + B$$
$$\text{Decay 2: } X \rightarrow C + D$$

Problem: The detector has different efficiencies for detecting particles A, B, C, and D. This makes directly calculating the branching ratios inaccurate.

$T(X \rightarrow AB) =$ True number, $D(X \rightarrow AB) =$ Detected number, $\varepsilon$ (A) etc.= Detection efficiencies

**Single Ratio:** The measured branching ratio of X decays would be:

$$\frac{D(X \rightarrow AB)}{D(X \rightarrow CD)} = \frac{\varepsilon(A) * \varepsilon(B) * T(X \rightarrow AB)}{\varepsilon(C) * \varepsilon(D) * T(X \rightarrow CD)}$$

Introducing a particle Y with similar decays and a known true branching ratio : R(Y) = $\frac{T(Y \rightarrow AB)}{T(Y \rightarrow CD)}$

**Double Ratio:**

$$\frac{D(X \rightarrow AB)/D(Y \rightarrow AB))}{D(X \rightarrow CD)/D(Y \rightarrow CD)}$$
$$= \frac{[\varepsilon(A)\varepsilon(B)T(X \rightarrow AB)]/[\varepsilon(A)\varepsilon(B)T(Y \rightarrow AB)]}{[\varepsilon(C)\varepsilon(D)T(X \rightarrow CD)]/[\varepsilon(C)\varepsilon(D)T(Y \rightarrow CD)]}$$

# Difference in Single ratio vs double ratio (0-10% centrality)

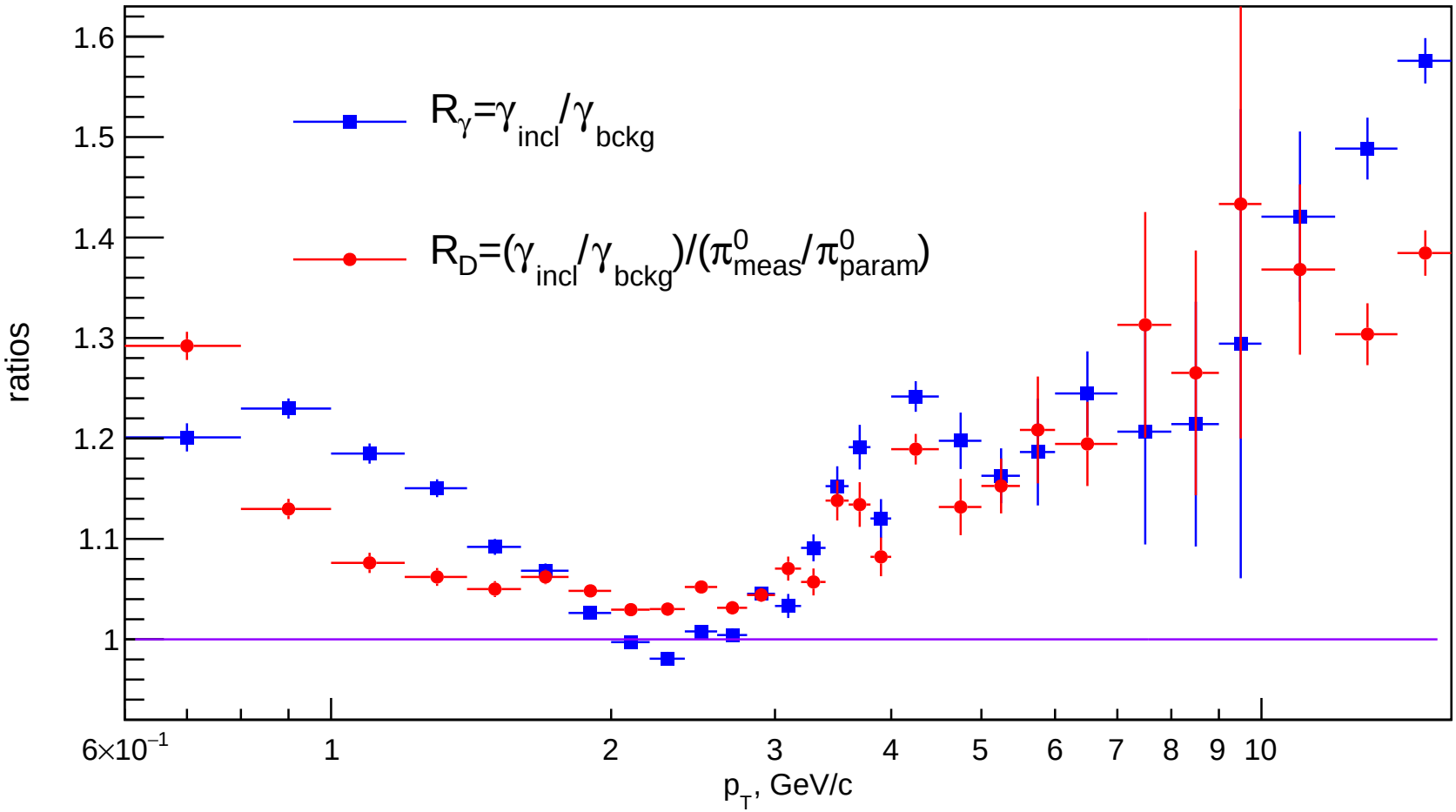

# Difference in shape of $\pi^0$ ratios from data and MC for centrality 0-10 %

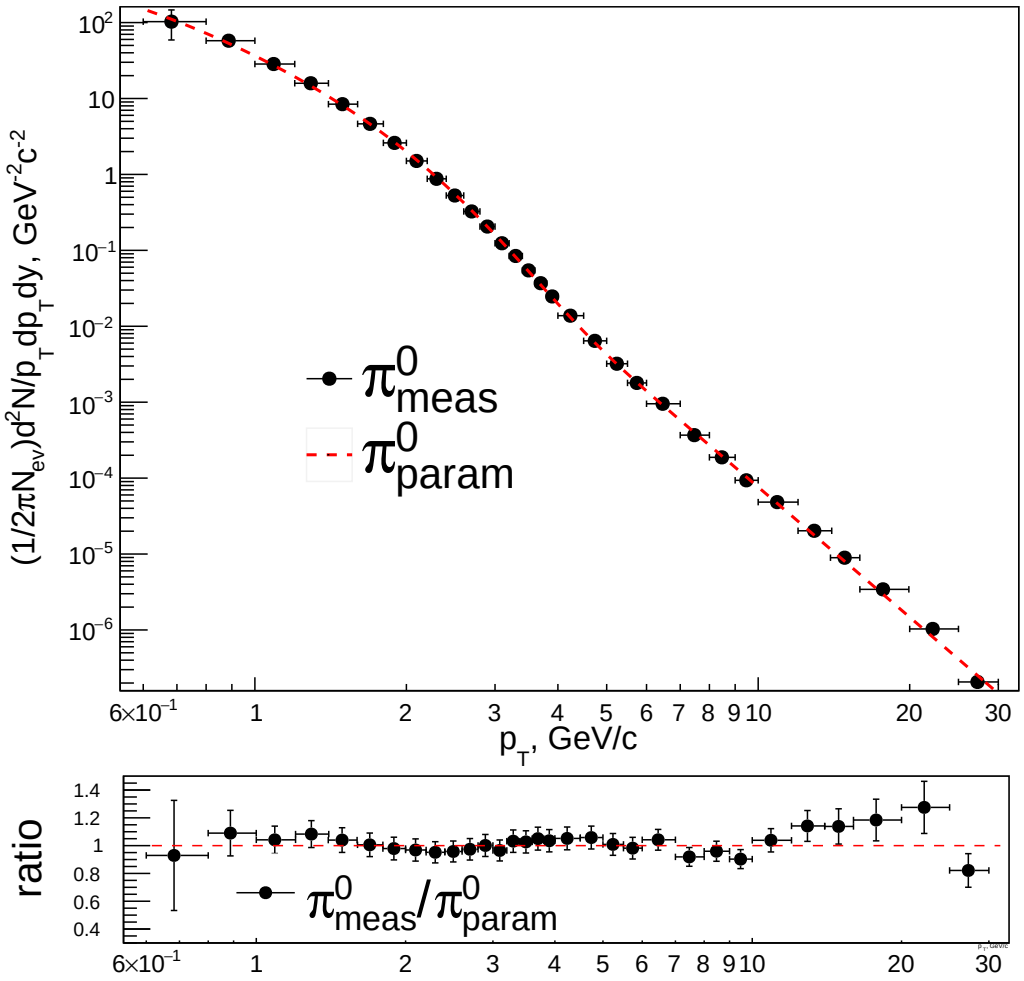

# Data Driven Approach and Photon embedding

- Data-driven approach (DDA):We define particle identification filters and the efficiency of the filters relative to different species of particles. It allows to build linear equation with the numbers of different particle clusters in each $p_T$-bin

- Embedding : We generate photons in the interaction point, model detector response and merge the obtained clusters from the Monte-Carlo event with those of the real events

$$
\begin{cases}
N_{cl} = & N_\gamma + N_{[\pi^\pm K^\pm]} + 2N_{[p\bar{p}]} + N_X, \\
N_{cl}^{CPV} = & C_\gamma^{CPV} N_\gamma + C_{\pi^\pm}^{CPV} N_{[\pi^\pm K^\pm]} + (C_{\pi^\pm}^{CPV} + C_\gamma^{CPV}) N_{[p\bar{p}]} + C_X^{CPV} N_X, \\
N_{cl}^{Disp} = & C_\gamma^{Disp} N_\gamma + C_{\pi^\pm}^{Disp} N_{[\pi^\pm K^\pm]} + 2C_{p\bar{p}}^{Disp} N_{[p\bar{p}]} + C_X^{Disp} N_X, \\
N_{cl}^{CPV+Disp} = & C_\gamma^{CPV} C_\gamma^{Disp} N_\gamma + C_{\pi^\pm}^{CPV} C_{\pi^\pm}^{Disp} N_{[\pi^\pm K^\pm]} + \\
& (C_{\pi^\pm}^{CPV} + C_\gamma^{CPV}) C_{p\bar{p}}^{Disp} N_{[p\bar{p}]} + C_X^{CPV} C_X^{Disp} N_X,
\end{cases}
$$

Figure: DDA, system of equations

# Elliptic flow : Previous results from PHENIX and ALICE

$$\frac{dN}{d\varphi} = \frac{N}{2\pi} \cdot (1 + \sum_{n>1} v_n cos(n[\varphi - \Psi_R]))$$

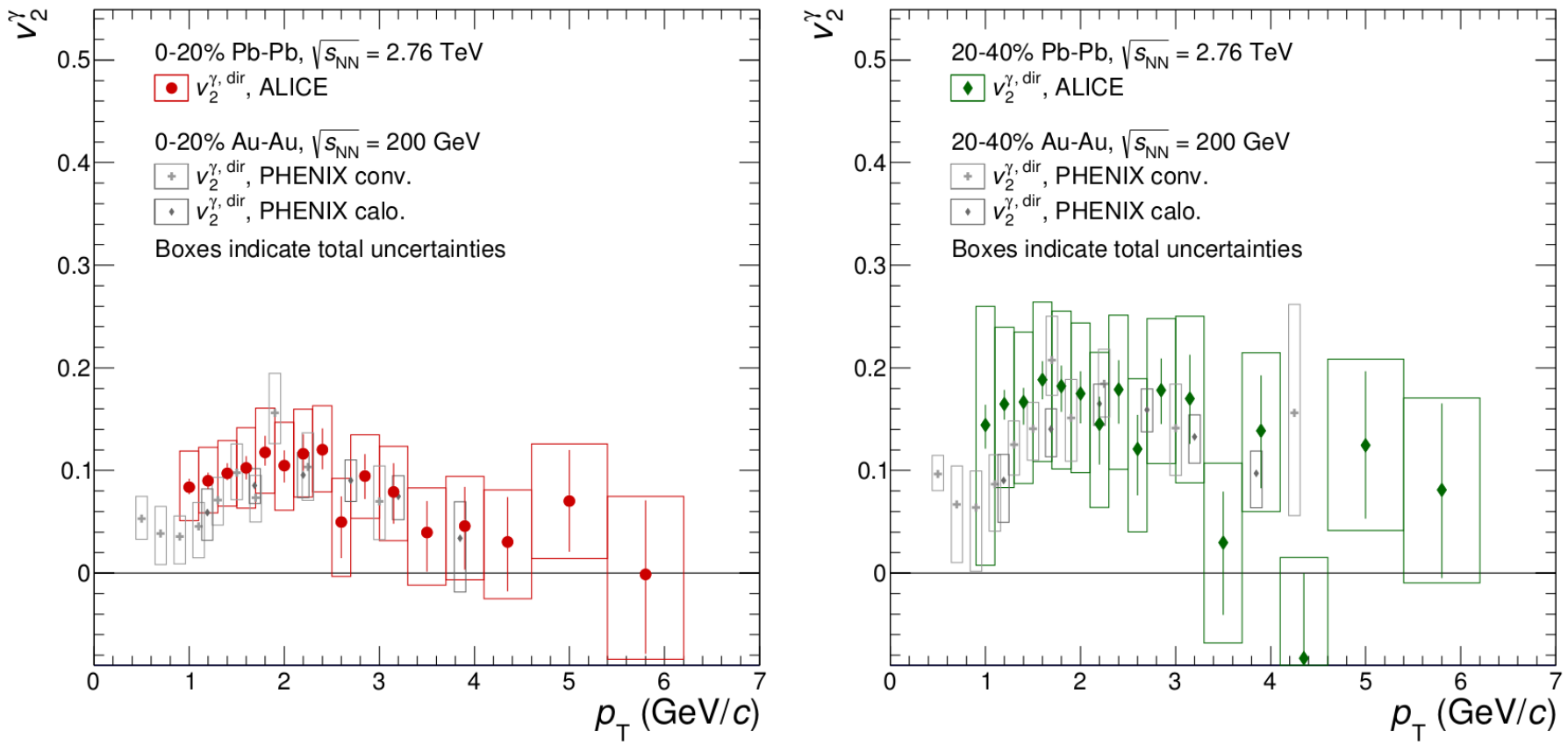


Figure: Elliptic flow of direct photons compared with PHENIX results for 0-20% (left) and 20-40% (right) centrality classes

[6] CERN-EP-2018-117

# Double ratio for p-p at $\sqrt{s} = 13$ TeV

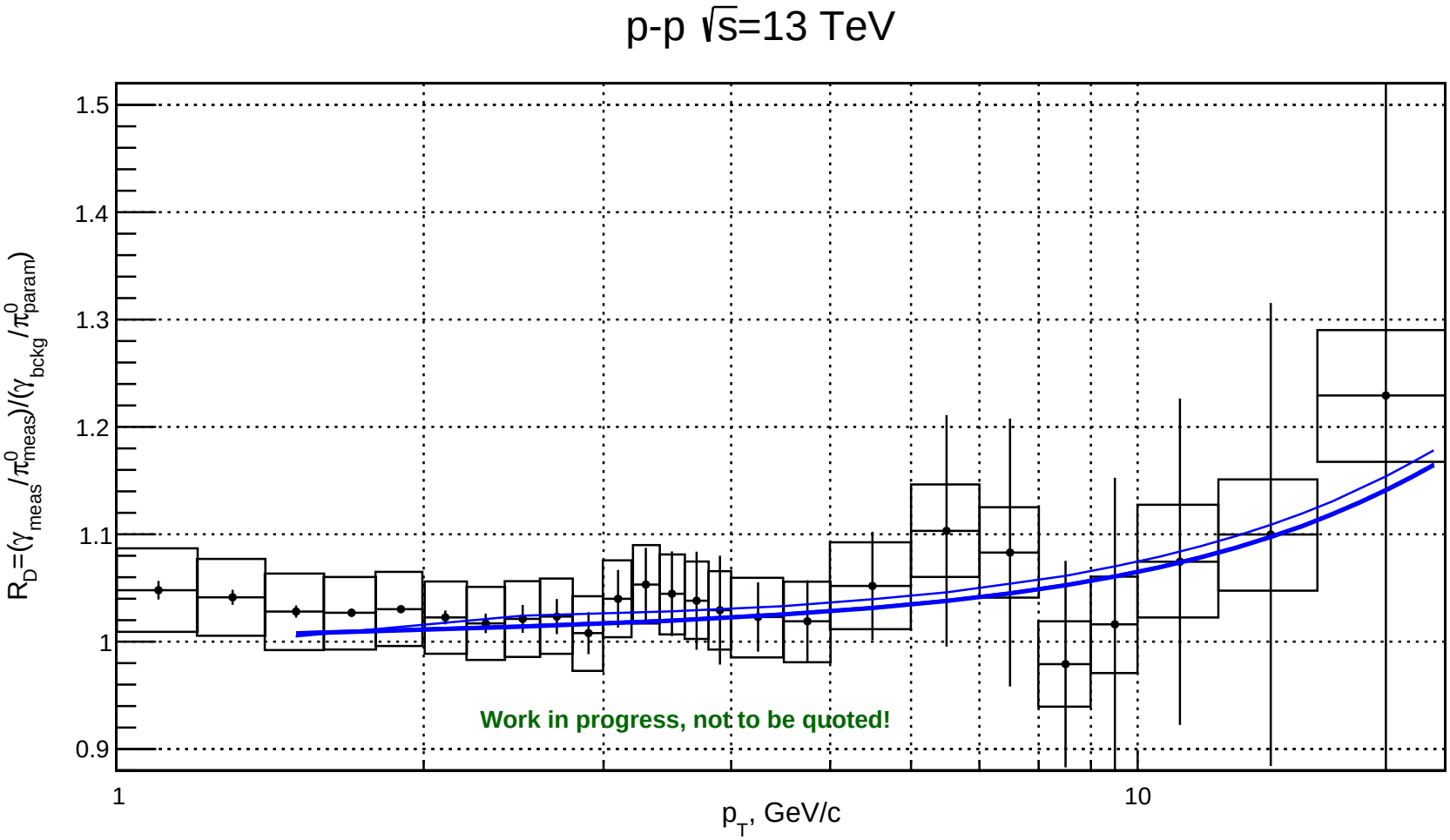


Figure: Double ratio for p-p collisions at $\sqrt{s} = 13$ TeV, statistical and systematic errors. The curves refer to the NLO pQCD predictions of prompt photon production for factorization scales $\mu_F = 0.5, 1, 2p_T$.

# Double ratio systematic uncertainties, centrality 0-10%

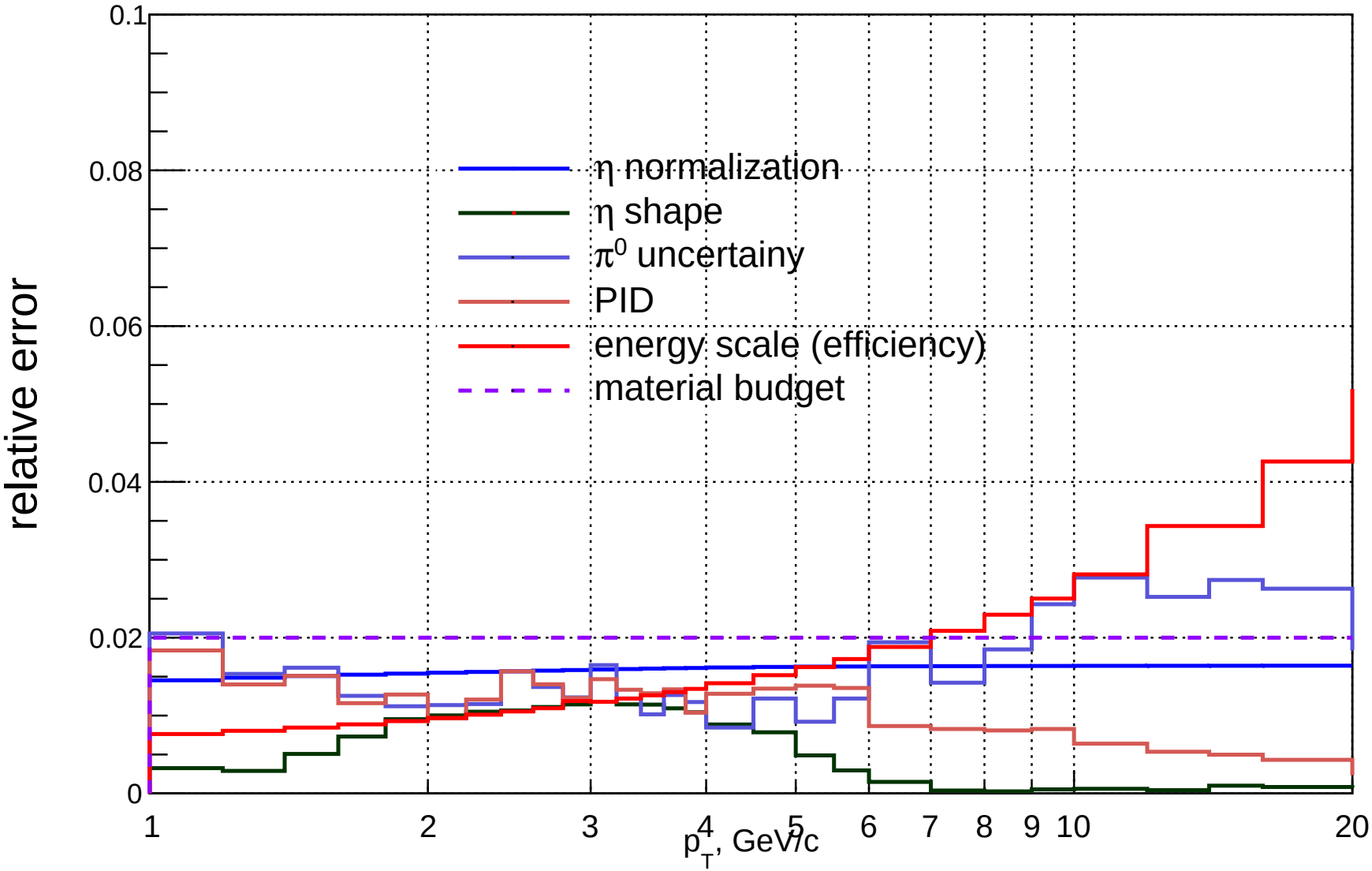

# Advantages of nucleus-nucleus(e.g. Au, Cu, Pb) collisions over p-p collisions in the study of QCD phase diagram and QGP

- Energy density:
  - p-p collisions: Typically a few GeV/fm$^3$
  - A-A collisions: 10-20 GeV/fm$^3$ or higher
- Temperature:
  - A-A collisions: Several hundred MeV to over a trillion degrees Kelvin
- Size and lifetime of the QGP:
  - p-p collisions: Highly transient and smaller in size
  - A-A collisions: Spatial extent of several femtometers, lasting tens to hundreds of femtoseconds
- Particle multiplicity:
  - A-A collisions: Significantly larger number of particles compared to p-p collisions
- Jet quenching:
  - A-A collisions: Much more pronounced, resulting in stronger energy loss and modification of jet-related observables

# Coordinate system in ALICE

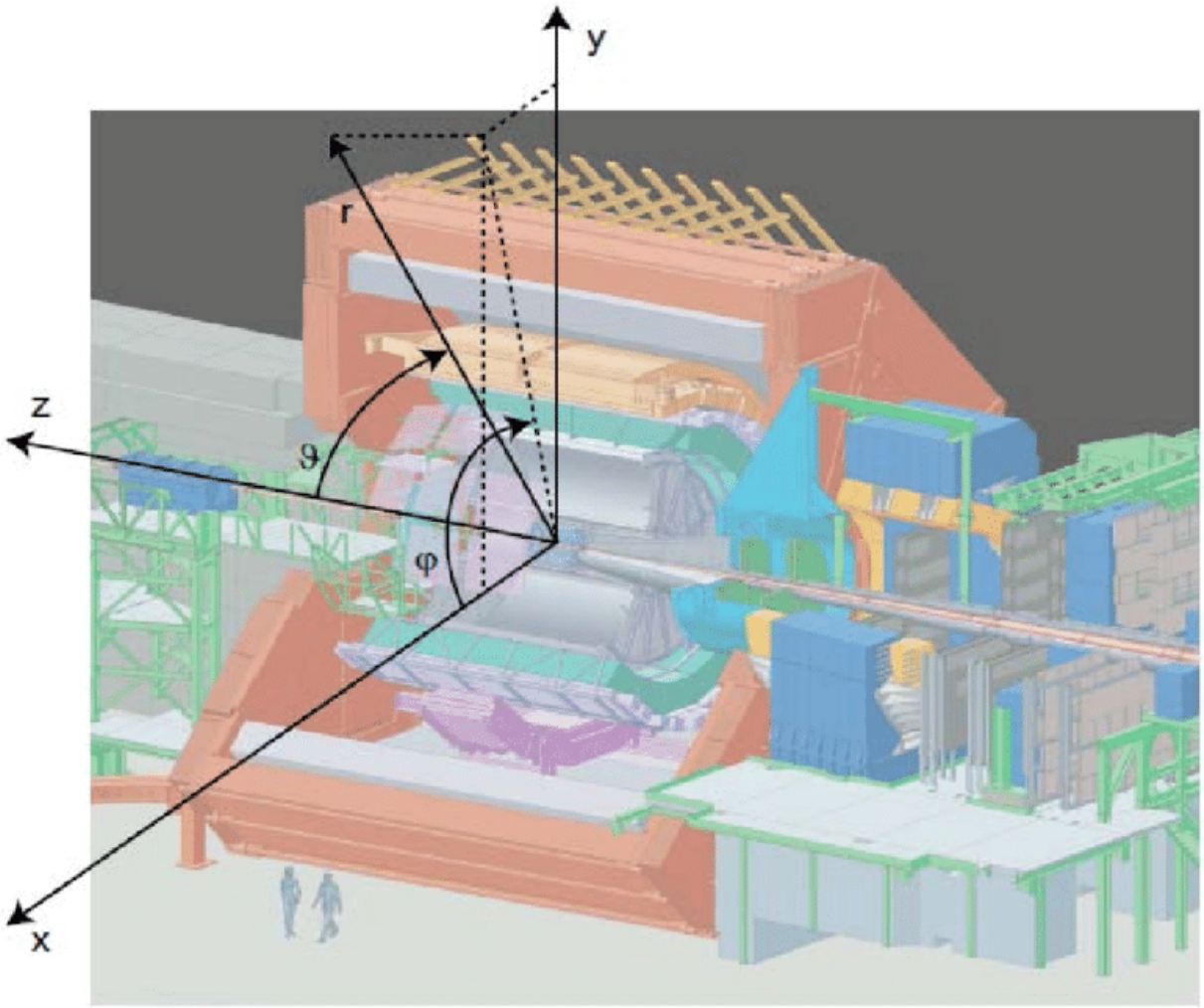


Figure: Like other major experiments at LHC, $(\theta, \phi, z)$ co-ordinate system is used at ALICE . Pseudo-rapidity $\eta = -ln(tan\frac{\theta}{2})$

[6] https://doi.org/10.1016/j.cpc.2021.108206